

# Energy-Efficient Resource Allocation and Trajectory Design for UAV Relaying Systems

Tong Zhang, Gongliang Liu, Haijun Zhang, *Senior Member, IEEE*, Wenjing Kang, George K. Karagiannidis, *Fellow, IEEE*, Arumugam Nallanathan, *Fellow, IEEE*

**Abstract**—Fuel-powered UAVs have long endurance of flight, heavy payload and adaptation to extreme environment. The mechanical operation and communication power are supported independently by fuel and batteries. In the paper, we study the energy efficiency of the communication system with a fuel-powered UAV relay. We consider a three-node communication network, consisting of a mobile relay, a source node, and a destination node. The UAV relay is able to change its 3-D trajectory to maintain high probability of LoS channels, receiving information from the fixed source node and transmitting it to the fixed destination node. The power allocation scheme and UAV's trajectory are designed to maximize the system energy efficiency, considering the constraints of speeds, UAV's altitudes, communication and mechanical energy consumption, the required data rates of the destination node and information-causality. We solve the power allocation sub-problem by splitting the domain of variables and transforming it into a convex optimization problem. And then a suboptimal scheme is provided to design the trajectory based on successive convex approximation method. Numerical results show the convergence of the proposed schemes and the performance of the proposed algorithms. The influences of time slots, constraints of fuel, communication power and required data rates are discussed.

**Index Terms**—Energy efficiency, power allocation, mobile relay, trajectory design.

## I. INTRODUCTION

Since relays were introduced to improve the communication performance, studies have been conducted to achieve better communication performance of communication systems [1]–[3]. Besides improving communication performance, mobile relays are efficient tools to deal with temporary and urgent communication missions [4]. By timely adjusting the

positions, mobile relays help to extend the communication coverage [5] and decrease outage probabilities [6].

In recent years, unmanned aerial vehicles (UAVs) have drawn substantial attention. Unlike other vehicles, the positions of which are constrained on the ground, the movement of aircraft is more adjustable. There are several ways to power UAVs, such as fuel, electricity and new energy sources [7]. Nowadays, electric UAVs are widely studied thanks to their economical costs and easy manipulation. However, one main drawback of electric UAVs lies on their limited endurance, i.e., less than 30 minutes. To lengthen UAVs' mission time, scientists proposed fuel cell-powered UAVs. A rotary-wing UAV equipped with a hydrogen cell can stay in the air for hours [8]. Nevertheless, as a prospective solution, the fuel cell-powered UAVs still need high budget and long start-up time [9]. Differently, internal combustion engine (ICE)-based UAVs, which are directly powered by fuel, have advantages like high load, long duration of flight, and adaptation to extreme environment, as well as drawbacks such as carbon dioxide pollution and noise [10]. Despite their disadvantages, fuel-powered UAVs still occupy important positions in agriculture [11] and military applications [12]. They are still irreplaceable in extreme environment or when heavy load is needed. And scientists are working on the development of engines and the exploration of new energy resources to improve the operation and control the pollution of fuel-powered UAVs [13], [14].

As for the UAVs' application in communication networks, UAVs can work as temporary base stations or relays [15]–[17]. Some researches emphasized the throughput of UAV-enabled relaying systems. In [18], the authors studied the data rate of a fixed-wing UAV-enabled relay, so as to achieve low outage probability when the UAV flew at a constant speed. In [19], the authors maximized the uplink rate by controlling the course angle of a UAV relay. Error rates and energy consumption were minimized for a UAV relay in [20]. In [21], the authors optimized the position of a UAV to communicate with several moving units on the ground.

Other applications, such as transmitting information for meteorological observations and broadcasting rescuing information in real time, can also be assisted by UAV relays. UAV relays have high mobility and can provide an approach of constructing communication after disasters and exploring unpopulated zones quickly. The long duration of UAV relays is necessary in a wild detecting or disaster rescuing scenario, because it is inconvenient to charge the batteries of UAVs frequently. Fuel powered UAVs become a possible choice. It's worth mentioning that fuel powered UAVs also need electric

This work is supported by National Key R&D Program of China (2019YFB1803304), the National Natural Science Foundation of China (61822104, 61771044), Beijing Natural Science Foundation (L172025, L172049), 111 Project (No. B170003), and the Fundamental Research Funds for the Central Universities (FRF-TP-19-002C1, RC1631), Beijing Top Discipline for Artificial Intelligent Science and Engineering, University of Science and Technology Beijing. The corresponding author is Haijun Zhang.

Tong Zhang is with Harbin Institute of Technology, Harbin, China, 150000 (e-mail: zhang7099@foxmail.com).

Gongliang Liu and Wenjing Kang are with Harbin Institute of Technology, Weihai, China, 264209 (e-mail: liugl@hit.edu.cn, kwjq@hit.edu.cn).

Haijun Zhang is with Beijing Advanced Innovation Center for Materials Genome Engineering, Institute of Artificial Intelligence, Beijing Engineering and Technology Research Center for Convergence Networks and Ubiquitous Services, University of Science and Technology Beijing, Beijing 100083, China (e-mail: haijunzhang@ieee.org).

George K. Karagiannidis is with Aristotle University of Thessaloniki, Thessaloniki, Greece (e-mail: geokarag@auth.gr).

Arumugam Nallanathan is with Queen Mary University of London, London, U.K. (e-mail: a.nallanathan@qmul.ac.uk).

batteries to power the communication module and other controlling modules. In addition, with their high mobility, UAVs have the advantage of providing line-of-sight (LoS) channels [22].

The trade-off between throughput and energy consumption, i.e., energy efficiency, has been widely studied in many communication scenarios [23]–[25]. It was mentioned that energy-efficiency problems of UAV relays are classified into two parts, energy-efficient mobility and energy-efficient communication [26]. The propulsion power of UAVs is much higher than the transmission power of the antennas, thus is regarded as the main influence on the energy consumption in electric UAVs [27]–[29].

Differently, on fuel-powered UAV relays, the energy efficiency of the communication module should be considered, because the ICE is powered separately by fuel, which has high energy density than batteries and can provide long time of energy supply [9]. To the best of the authors' knowledge, few researches have been conducted on energy-efficient communication of fuel-power-UAV relaying systems. Fuel-powered UAVs also need batteries for communication module. The batteries could be independent or rechargeable. Rechargeable batteries can be powered by the engine kinetic energy or solar power. Because of these conditions, the challenges of studying fuel-powered UAV communication lies on two types of energy supply, which makes the designing of the communication schemes more complicated. In this paper, we study the energy efficiency communication of a UAV relay. The UAV's 3-D movement was deployed to maintain high probability of LoS channels. We also guarantee the data rate of destination node above a certain level. The mechanical energy consumption is considered as a constraint, set according to the amount of fuel reserved for the period of communication.

### A. Contributions

In this paper, we study a fuel-powered UAV relay. The relay establishes temporary communication for two nodes on the ground, between which the communication is blocked. The relay adjusts its 3-D trajectory to amplify and forward information from the source node to the destination node. The source node and the mobile relay can both adjust their power allocation schemes. Considering the data rate of the destination node, the power consuming constraints and the mobility features of the relay, the energy efficiency maximization problem is formulated. We solve the non-convex problem by dealing with power allocation and the trajectory separately.

The contributions of this paper are as follow:

- *Maximizing the energy efficiency of the communication module of a fuel-powered UAV relay:* The key difference between fuel-powered UAVs from battery-powered UAVs is independent energy supplies for operation and communication. In this paper, we consider the energy-efficiency of the communication module on a fuel-powered UAV relay. The fuel consumption is constrained and the data rate of the destination node is guaranteed above a threshold.
- *Optimal solution for the power allocation scheme:* We propose a novel energy efficient power allocation scheme

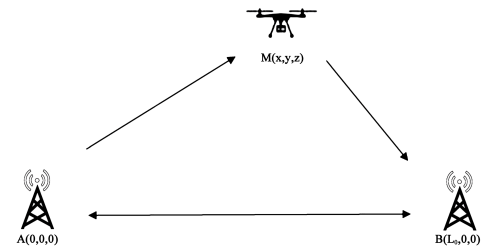


Fig. 1. A rotary-wing UAV relay in a three-node communication system.

under a total energy consumption constraint and information causality constraints. The power allocations for both the source node and the relay are optimized. By discussing the bounds of the feasible domain, we transfer the non-convex problem into a convex optimization problem.

- *Designing the 3-D relay trajectory of the UAV:* We study the positions and speeds of the relay at all time slots in order to maximize the system energy efficiency as well as to ensure wanted data rate for the destination node. The UAV's mobility is deployed to maintain high probability of LoS channels. The mechanical energy consumption of the UAV is constrained by the fuel supply. We use slake variables and successive convex approximation method to obtain a suboptimal solution for the UAV trajectory.

### B. Paper Organization

We organize the rest of the paper in six sections. In Section II, the system is formulated in a mathematical model. In Section III, we optimize the power allocation for given trajectory. In Section IV we design the trajectory of the relay using successive convex approximation method. In Section V, the iterative algorithm is proposed to solve the joint problem. The convergence and complexity of the proposed algorithm are discussed. In Section VI, we present simulation results to demonstrate the performance of the proposed algorithm. The influence of length of time slots, fuel supply, communication energy and required data rates are discussed. Section VII includes the conclusion of the paper.

## II. PROBLEM FORMULATION

### A. System Model

In our system, we consider a three node communication system, the relay in which is a fuel-powered rotary-wing UAV. We assume that the nodes work in orthogonal frequency bands, and are not interfered by each other. The UAV relay, denoted as M, amplifies and forwards the received information from the source node A to the destination node B. As shown in Fig. 1, A and B are fixed on the ground. We assume that they cannot communicate directly because of topographic reasons, and they are  $L_0$  meters away from each other. The buffer of M is large enough to store the received data during the communication. To study the continuous communication

process, we divide the time of communication  $T$  into  $K$  slots. Denote the length of a time slot as  $\Delta t$ , we have

$$T = K\Delta t. \quad (1)$$

The time slot should be small so that the change of the UAV's positions during a time slot is much shorter than the distance of the UAV to the ground users. We use the positions of the UAV at the beginning or the end of the time slots to compute the data rates during the time slot. When there are  $K$  time slots from 1 to  $K$ , there will be  $K + 1$  sampling nodes of time between and on the two sides of all time slots, denoted as  $k = 0, \dots, K$ . When referring to positions of the UAV, subscript  $k$  indicates the  $k$ th node of time. When referring to speeds, the subscript  $k$  means the average speed during the  $k$ th time slot, i.e., the period between the  $(k - 1)$ th and the  $k$ th time nodes. At the  $k$ th node of time, the position of the relay is  $(x_k, y_k, z_k)$ . The positions of A and B are  $(0, 0, 0)$  and  $(L_0, 0, 0)$  respectively. The distance between A and M and M and B are

$$l_{AM,k} = \sqrt{x_k^2 + y_k^2 + z_k^2}, \quad (2)$$

and

$$l_{MB,k} = \sqrt{(L_0 - x_k)^2 + y_k^2 + z_k^2}, \quad (3)$$

respectively.

### B. Channel Model

Since the strength of air-to-ground (A2G) channel is the high probability of line-of-sight (LoS) [19], UAV-enabled communication is helpful to transmit high frequency signals, which suffer from significant attenuation in non-line-of-sight (NLoS) channels. Referring to the probability LoS model in recommendation document by the International Telecommunication Union (ITU) [30], the probability of LoS is related to parameters of circumstances, i.e., construct area proportions, building quantities and heights. There is a precise approximation of the ITU model raised in [31] which is widely used in studies considering A2G channels [32]–[35]. Referring the LoS probability model [31], the possibility of LoS can be written as a Sigmoid function of the angle of elevation,

$$P_{LoS}(\eta) = \frac{1}{1 + \alpha_0 \exp[-\beta_0(\eta - \alpha_0)]}, \quad (4)$$

where  $\alpha_0$  and  $\beta_0$  are S-curve parameters, different in suburban, urban and dense urban environments.  $\eta$  is the elevation angle of the A2G channel. The LoS probabilities versus elevation angles are shown in Fig. 2.

Considering the large-scale fading effects  $h_l$  and the small-scale fading effects  $h_s$  of the A2G channel, the channel model at time  $k$  is formulated as

$$H = h_l h_s. \quad (5)$$

The large scale fading for the A2G channel model is represented as

$$|h_l|^2 = \begin{cases} C_{LoS} l^{-\alpha_L}, & P_{LoS}(\eta) \\ C_{NLoS} l^{-\alpha_N}, & 1 - P_{LoS}(\eta), \end{cases}$$

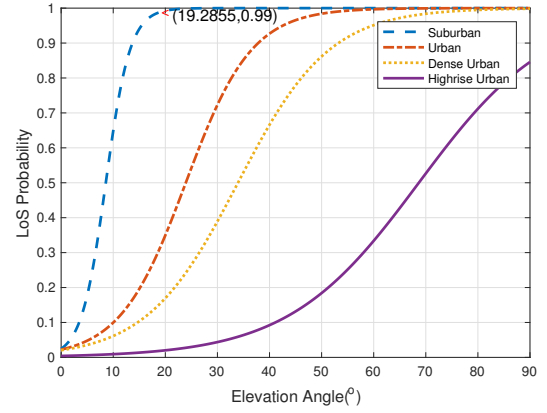


Fig. 2. The LoS probability in suburban, urban, dense urban and high-rise urban.

where  $C_{LoS}$  and  $C_{NLoS}$  are the path loss parameters for LoS and NLoS channels respectively.  $\alpha_L$  and  $\alpha_N$  are path-loss exponents for LoS and NLoS channels, respectively, usually ranging from 2 to 6.

The average received signal to noise ratio (SNR) is expressed as

$$\mathbb{E}[SNR_k] = \mathbb{E}\left[\frac{p_t |H_k|^2}{N_0 B}\right] = \frac{p_t \mathbb{E}[|H_k|^2]}{N_0 B}, \quad (6)$$

where  $B$  is the bandwidth,  $p_t$  is the communication power from the transmitter A or M.  $N_0$  is the noise power spectral density. Then the received data rate is

$$R_k = B \log_2 \left(1 + \frac{p_t \mathbb{E}[|H_k|^2]}{N_0 B}\right). \quad (7)$$

For simplicity of presentation, we use the average data rate per reference bandwidth  $R_k/B$ . Since the small-scale fading coefficient is independent with the large scale fading coefficient, using property of small-scale fading that

$$\mathbb{E}[|h_s|^2] = 1, \quad (8)$$

we have

$$\begin{aligned} \mathbb{E}[|H_k|^2] &= P_{LoS}(\eta) C_{LoS} l^{-\alpha_L} + P_{NLoS}(\eta) C_{NLoS} l^{-\alpha_N} \\ &= \left[ P_{LoS}(\eta) + (1 - P_{LoS}(\eta)) \frac{C_{NLoS} l^{-(\alpha_N - \alpha_L)}}{C_{LoS}} \right] C_{LoS} l^{-\alpha_L} \\ &\approx C_{LoS} l^{-\alpha_L} \end{aligned} \quad (9)$$

$P_{LoS}(\eta) + (1 - P_{LoS}(\eta)) \frac{C_{NLoS} l^{-(\alpha_N - \alpha_L)}}{C_{LoS}}$  is approximated to be 1 [36]–[38]. The approximation makes sense when  $P_{LoS}$  is high enough and the signal power from the NLoS channel is negligible. For instance, when the elevation angle is larger than  $20^\circ$ , the LoS probability is higher than 99% in suburban area.  $C_{NLoS}$  is smaller compared to  $C_{LoS}$ , and also  $\alpha_N$  is usually higher than  $\alpha_L$ , making the NLoS power even smaller. To maintain LoS channels for the communication, we set that the altitude  $z_k, k = 0, \dots, K$ , should satisfy

$$\frac{z_k}{l_{AM,k}} \geq \sin \eta, \quad \frac{z_k}{l_{MB,k}} \geq \sin \eta. \quad (10)$$

where  $\eta$  is the constraint of elevation angle, large enough to maintain LoS channels with probability one for the communication of A to M and M to B. The UAV starts to work after its altitude satisfies (10). Here we need to mention that for a deeper investigation, the accurate channel model and data rates related to elevation angles are momentous but quite complicated, and are left as future work.

### C. Mechanical Energy Consumption

The mechanical energy consumption of aircrafts is calculated according to the trim condition of the force during the flight [39]. We assume that the UAV moves with nearly constant speed in each time slot. The acceleration power can be omitted when the acceleration is small and the time of acceleration is much shorter than the time of steadily flying [40]. Denote the level component of the UAV's speed as  $v_{l,k}$ , the vertical speed as  $v_{c,k}$ . The total mechanical power in time slot  $k$  is [39]–[41]

$$P_{total,k}(v_{l,k}, v_{c,k}) = (1+c) \frac{W^{3/2}}{\sqrt{2\rho A}} \sqrt{\sqrt{1 + \frac{v_{l,k}^4}{4v_h^4}} - \frac{v_{l,k}^2}{2v_h^2}} + \frac{\delta \rho S_{blade} v_{tip}^3}{8} \left(1 + \frac{3v_{l,k}^2}{v_{tip}^2}\right) + \frac{r_d \rho S_{blade} v_{l,k}^3}{2} + W v_{c,k}, \quad (11)$$

where  $W$ ,  $\rho$  and  $A$  are the weight of the aircraft, the density of air and the area of rotor disc, respectively.  $c$  is the incremental correction factor.  $v_h$  is the induced velocity in hovering state.  $\delta$  is the profile drag coefficient.  $\rho$  is the density of the air.  $S_{blade}$  is the total blade area.  $v_{tip}$  is the speed of the rotor blade tip.  $r_d$  is the fuselage drag ratio.

The fuel consumption is

$$m_f = \frac{\sum_{k=1}^K P_{total,k} \Delta t}{c_p \eta_{fuel}}, \quad (12)$$

where  $c_p$  and  $\eta_{fuel}$  are the heat of combustion of the fuel and average thermodynamic efficiency of the gas turbine respectively. Note that along with the burning of fuel, the weight of the aircraft decreases. This influence is usually considered in studying the persistence of a fuel-powered aircraft [39] by solving (12) as a differential equation. In our model, we assume that the weight of UAV keeps stable during a short period. This is reasonable because, for instance, for a 17-Kg UAV with an average fuel consumption of 4000cc/h, the weight loss after flying for 10 minutes is less than 3% of the total weight of the UAV. When the model is applied to much longer duration, one may refer to the UAV's handbook and use the empiric number to estimate the average fuel consumption and update the UAV's weights. As for the mobility of the UAV, the speed at horizontal projection in time slot  $k$  is

$$v_{l,k} = \sqrt{(x_{k+1} - x_k)^2 + (y_{k+1} - y_k)^2} / \Delta t. \quad (13)$$

The vertical speed at  $k$  is

$$v_{c,k} = (z_{k+1} - z_k) / \Delta t. \quad (14)$$

### D. System Energy Efficiency

Based on the A2G channel and fuel consumption problems discussed in subsections A, B and C, we formulate the problem of maximizing the average energy efficiency during each time slot as

$$\max_{\substack{\{p_A, p_M\} \\ \{x, y, z\}}} \frac{1}{K} \sum_{k=1}^K \log_2 \left[ 1 + \frac{p_{M,k} C_{LoS}}{l_{MB,k}^\alpha N_0 B} \right], \quad (P1)$$

$$\text{s.t. } \frac{z_k}{l_{AM,k}} \geq \sin \eta, \frac{z_k}{l_{MB,k}} \geq \sin \eta, \forall k \quad (15a)$$

$$I_{MB,k} \leq I_{AM,k-1}, k = 1, \dots, K, \quad (15b)$$

$$\Delta t \left( \sum_{k=0}^{K-1} p_{A,k} \right) \leq E_A, \quad (15c)$$

$$\Delta t \left( \sum_{k=1}^K p_{M,k} \right) \leq E_M, \quad (15d)$$

$$R_{MB,k} \geq R_0, k = 1, \dots, K, \quad (15e)$$

$$p_{A,k} \geq 0, p_{M,k} \geq 0, \forall k, \quad (15f)$$

$$v_{l,k} \leq v_0, k = 1, \dots, K, \quad (15g)$$

$$v_{c,k} \leq v_c, k = 1, \dots, K, \quad (15h)$$

$$\sqrt{(v_{l,k+1} - v_{l,k})^2 + (v_{c,k+1} - v_{c,k})^2} \leq a_{max} \Delta t, k = 1, \dots, K-1, \quad (15i)$$

$$H_{min} \leq z_k \leq H_{max}, \forall k, \quad (15j)$$

$$m_f \leq m_0. \quad (15k)$$

In (P1),  $p_c$  is the circuit power consumption of the communication module.  $p_A$  and  $p_M$  denotes the communication power forwarded by A and M. (15a) and (15j) are the constraints of the UAV's heights. (15b) are information causality constraints.  $I_{AM,k}$  and  $I_{MB,k}$  are

$$I_{AM,k} = \sum_{i=0}^k \Delta t B \log_2 \left( 1 + \frac{p_{A,i} C_{LoS}}{l_{AM,k}^\alpha N_0 B} \right), \quad (16)$$

$$I_{MB,k} = \sum_{i=1}^k \Delta t B \log_2 \left( 1 + \frac{p_{M,i} C_{LoS}}{l_{MB,k}^\alpha N_0 B} \right), \quad (17)$$

respectively. Note that considering the processing time of the UAV relay as well as for simplicity of computation, we use the positions at the beginning of time slot  $k$  to compute  $l_{AM,k-1}$  and  $R_{AM,k-1}$ , and we use the position at end of time slot  $k$  to compute  $l_{MB,k}$  and  $R_{MB,k}$ . Thus we have  $R_{AM,k}, k = 0, \dots, K-1, R_{MB,k}, k = 1, \dots, K$  [38]. Here the subscripts  $k$  of  $R_{AM}$  and  $R_{MB}$  are corresponding to  $l_{AM}$  and  $l_{MB}$ . For concision, we omit  $\Delta t B$  in (16) and (17) in the following discussion.

Since one of the main differences between fuel-powered UAVs and battery-powered UAVs is that direct-fuel-driven UAVs have independent power supplies for propulsion and communication. The energy consumption of the UAV relay not only depends on the communication module, but is also related to the amount of fuel. Constraints (15c) and (15d) represent the communication energy, supplied by the battery, and constraint (15k) means the limitation of the fuel consumption. (15e) is to guarantee the required data rate of the receiving node. (15g)

and (15h) give the maximum level and vertical speeds. (15i) is the constraint of acceleration.

Note that (P1) is non-convex due to the non-convex objective function and non-convex constraints (15a), (15b), (15e) and (15k). To solve (P1), we decouple the problem into two parts: communication power arrangement for A and M and trajectory design of the UAV. For simplicity,  $1/K$  in the objective function of (P1) is omitted in the following illustration.

### III. POWER ALLOCATION FOR FIXED RELAY TRAJECTORY

Firstly, in this section, we need to clarify that  $x \in [\cdot]$  means  $x$  belongs to the closed interval  $[\cdot]$ . When the trajectory of the relay is given,  $x_k, y_k, z_k$  are fixed, and  $l_{AM,k}$  and  $l_{MB,k}$  are fixed. Denote  $|H_{AM,k}|^2 = C_{LoS}/l_{AM,k}^\alpha$ , we write  $p_{A,k}$  as a function of  $R_{AM,k}$ :

$$p_A(R_{AM,k}) = \frac{(2^{R_{AM,k}} - 1) N_0 B}{|H_{AM,k}|^2}. \quad (18)$$

Similarly, according to (7), denote  $|H_{MB,k}|^2 = C_{LoS}/l_{MB,k}^\alpha$ , the relationship between  $p_{M,k}$  and  $R_{MB,k}$  can be written as

$$p_M(R_{MB,k}) = \frac{(2^{R_{MB,k}} - 1) N_0 B}{|H_{MB,k}|^2}. \quad (19)$$

Then, the power allocation sub-problem is formulated as:

$$\begin{aligned} \max_{R_{AM,k}, R_{MB,k}} \quad & \sum_{k=1}^K \frac{R_{MB,k}}{p_M(R_{MB,k}) + p_c}, \\ \text{s.t.} \quad & (15b)-(15f). \end{aligned} \quad (P2)$$

The objective function of (P1) is non-concave. To solve (P1), we analyse the convex property of the objective function by splitting the feasible region of the variables. First of all, we define

$$E(R_{MB,k}) = \frac{R_{MB,k}}{p_M(R_{MB,k}) + p_c}, \quad (21)$$

$$E(\mathbf{R}_{MB}) = \sum_{k=1}^K E(R_{MB,k}). \quad (22)$$

Although  $E(R_{MB})$  is strictly quasi-concave, the prove of which is shown in Appendix A, the sum of several quasi-concave functions is not guaranteed to be quasi-concave. To identify the convex properties of  $E(R_{MB})$ , we look at its first-order derivative.

$$\frac{\partial E(R_{MB})}{\partial R_{MB,k}} = \frac{p_c + p_M(R_{MB,k}) - R_{MB,k} \cdot p'_M(R_{MB,k})}{(p_M(R_{MB,k}) + p_c)^2}, \quad (23)$$

where  $p'_M(R_{MB,k})$  is the first derivative of  $p_M(R_{MB,k})$ . Denote the numerator of (23) as  $\beta(R_{MB,k})$

$$\beta(R_{MB,k}) = p_c + p_M(R_{MB,k}) - R_{MB,k} \cdot p'_M(R_{MB,k}). \quad (24)$$

**Lemma 1:**  $\beta(R_{MB,k})$  has a unique positive root. Denote the root of  $\beta(R_{MB,k})$  as  $\tilde{R}_{MB,k}$ ,

$$\beta(\tilde{R}_{MB,k}) = 0. \quad (25)$$

It can be proved that  $\tilde{R}_{MB,k} > 0$  and

$$\begin{cases} \beta(R_{MB,k}) > 0, & 0 < R_{MB,k} < \tilde{R}_{MB,k}, \\ \beta(R_{MB,k}) < 0, & R_{MB,k} > \tilde{R}_{MB,k}. \end{cases}$$

*Proof:* Please refer to Appendix B. ■

According to Lemma 1, we find that for  $R_{MB,k} < \tilde{R}_{MB,k}$ ,  $E(R_{MB,k})$  is monotonically increasing, and for  $R_{MB,k} > \tilde{R}_{MB,k}$ ,  $E(R_{MB,k})$  is monotonically decreasing. Using the dichotomy method,  $\tilde{R}_{MB,k}$  can be solved. Splitting the feasible region of (P2) at  $\tilde{R}_{MB,k}$ , we find Lemma 2.

*Lemma 2:*

$$E(R_{MB,k}) \text{ is } \begin{cases} \text{concave, } R_{MB,k} \leq \tilde{R}_{MB,k} \\ \text{monotonically decreasing, } R_{MB,k} > \tilde{R}_{MB,k} \end{cases}$$

*Proof:* Please refer to Appendix C. ■

$R_0$  is the constraint for the minimum data rate required by the destination node. We compare  $\tilde{R}_{MB,k}$  with  $R_0$  and find that:

a): if  $\tilde{R}_{MB,k} \leq R_0$ ,  $E(R_{MB,k})$  is monotonically decreasing, because  $\tilde{R}_{MB,k}$  should be larger than  $R_0$  and thus is larger than  $\tilde{R}_{MB,k}$ .

b): if  $\tilde{R}_{MB,k} > R_0$ , we have

$$E(R_{MB,k}) \text{ is } \begin{cases} \text{concave, } R_0 \leq R_{MB,k} \leq \tilde{R}_{MB,k} \\ \text{monotonically decreasing, } R_{MB,k} > \tilde{R}_{MB,k} \end{cases}$$

Since for different time slots, the UAV's positions may change, thus the channel coefficients are different. There might be some  $\tilde{R}_{MB,k}$  satisfying condition a) and others satisfying b). We denote the "k" in  $\tilde{R}_{MB,k}$  with condition a) as  $k = a$ , while the "k" with condition b) as  $k = b$ . Denote the optimal solution for (P2) as  $\mathbf{R}_{MB}^*$ , representing  $\{R_{MB,k}^*\}_{k=1}^K$ .

**Theorem 1:**  $R_{MB,a}^* = R_0$ ,  $R_{MB,b}^* \in [R_0, \tilde{R}_{MB,b}]$ .

*Proof:* Please refer to Appendix D. ■

Theorem 1 means that after solving  $\tilde{R}_{MB,k}$ , we can identify  $k = a$ , and get the optimal  $R_{MB,a} = R_0$  directly. The work left is solving  $R_{MB,b}^*$ . Note that  $E(R_{MB,b})$  is concave for  $R_{MB,b} \leq \tilde{R}_{MB,b}$ . Then we rewrite (P2) as (P2')

$$\max_{R_{AM,n}, R_{MB,b}} \sum_a \frac{R_0}{p_M(R_0) + p_c} \quad (P2')$$

$$+ \sum_b \frac{R_{MB,b}}{p_M(R_{MB,b}) + p_c},$$

$$\text{s.t. } I_{MB,a}^k + I_{MB,b}^k \leq I_{AM,k-1}, k=1, \dots, K, \quad (26a)$$

$$\sum_{k=0}^{K-1} p_A(R_{AM,k}) \leq E_A, \quad (26b)$$

$$\sum_a p_M(R_0) + \sum_b p_M(R_{MB,k}) \leq E_M, \quad (26c)$$

$$R_0 \leq R_{MB,b} \leq \tilde{R}_{MB,b}, \quad (26d)$$

$$R_{AM,k} \geq 0, \forall k, \quad (26e)$$

where  $I_{MB,a}^k = \sum_{a \in [1,k]} R_0$ , and  $I_{MB,b}^k = \sum_{b \in [1,k]} R_{MB,b}$ .  $a$  and  $b$  are both integers.

**Property 1:** (P2') is a convex optimization problem.

*proof:* We have proved in Appendix C that  $E(R_{MB,k})$  is concave for  $R_0 \leq R_{MB,b} \leq \tilde{R}_{MB,b}$ . The objective

function of (P2) is the sum of a constant  $\sum_a \frac{R_0}{p_M(R_0)+p_c}$  and some concave functions  $\sum_b \frac{R_{MB,b}}{p_M(R_{MB,b})+p_c}$ . Since adding is a convexity preserving operation, the objective function of (P2') is concave. Obviously, constraints (26a)-(26e) are convex constraints. So (P2') is a convex optimization problem. ■

The optimal data rates of  $a$  can be solved without operating the iterative procedure, and the number of independent variables of (P2) has been reduced from  $2K$  to  $K+B$ , where  $B$  is the number of  $b$ .

The convex problem (P2') can be solved using Lagrange Multiplier Method. Let  $\lambda_k, k = 1, \dots, K, \zeta$  and  $\xi$  represent Lagrange dual variables. The Lagrangian dual function of (P2') is

$$\begin{aligned} L(\{\mathbf{R}_{AM}, \mathbf{R}_{MB,b}\}, \{\boldsymbol{\lambda}, \zeta, \xi\}) &= \sum_a \frac{R_0}{p_M(R_0)+p_c} + \sum_b \frac{R_{MB,b}}{p_M(R_{MB,b})+p_c} \\ &+ \sum_{k=1}^K \lambda_k (I_{AM,k-1} - I_{MB,a}^k - I_{MB,b}^k) \\ &+ \zeta \left[ E_A - \sum_{k=0}^{K-1} p_A(R_{AM,k}) \right] \\ &+ \xi \left[ E_M - \sum_a p_M(R_0) - \sum_b p_M(R_{MB,b}) \right], \end{aligned} \quad (27)$$

In each iteration  $j$ , after giving the dual variables, update  $R_{AM,k}$  and  $R_{MB,b}$  to maximize  $L(\{\mathbf{R}_{AM}, \mathbf{R}_{MB,b}\}; \{\boldsymbol{\lambda}, \zeta, \xi\})$  by solving

$$\frac{\partial L(\{\mathbf{R}_{AM}, \mathbf{R}_{MB,b}\}; \{\boldsymbol{\lambda}, \zeta, \xi\})}{\partial R_{AM,k}} = 0, \quad (28)$$

$$\frac{\partial L(\{\mathbf{R}_{AM}, \mathbf{R}_{MB,b}\}; \{\boldsymbol{\lambda}, \zeta, \xi\})}{\partial R_{MB,b}} = 0. \quad (29)$$

Then we have

$$R_{AM,k}^j = \max \left[ 0, \log_2 \left( \frac{\sum_{i=k}^K \lambda_i |H_{AM,k}|^2}{\zeta N_0 B \ln 2} \right) \right], k = 1, \dots, K, \quad (30)$$

where  $R_{AM,k}^j$  is the updated  $R_{AM,k}$  after the  $j$ th iteration. The analytical solution of (29) is hard to derive, but

$$\begin{aligned} &\frac{\partial L(\{\mathbf{R}_{AM}, \mathbf{R}_{MB,b}\}; \{\boldsymbol{\lambda}, \zeta, \xi\})}{\partial R_{MB,b}} \\ &= \frac{\beta(R_{MB,b})}{(p_M(R_{MB,b})+p_c)^2} - \sum_{i=b}^K \lambda_i - \xi p_M'(R_{MB,b}) \end{aligned} \quad (31)$$

is monotonically decreasing. This can be proved by looking at the second-order derivative:

$$\begin{aligned} &\frac{\partial^2 L(\{\mathbf{R}_{AM}, \mathbf{R}_{MB,b}\}; \{\boldsymbol{\lambda}, \zeta, \xi\})}{\partial^2 R_{MB,b}} \\ &= \frac{\partial^2 E(R_{MB,b})}{\partial R_{MB,b}^2} - \xi p_M''(R_{MB,b}). \end{aligned} \quad (32)$$

In Appendix C, we have proved that  $\frac{\partial^2 E(R_{MB,b})}{\partial R_{MB,b}^2}$  is negative.  $\xi$  and  $p_M''(R_{MB,b})$  are both positive. Thus the second-order derivative of  $L(\{\mathbf{R}_{AM}, \mathbf{R}_{MB,b}\}; \{\boldsymbol{\lambda}, \zeta, \xi\})$  about  $R_{MB,b}$  is

negative. Let  $R_{MB,b}^+$  denote the root of (29). Denote  $R_{MB,b}^j$  as the updated  $R_{MB,b}$  after the  $j$ th iteration, we can update  $R_{MB,b}^j$  by

$$R_{MB,b}^j = \max [R_{MB,b}^+, R_0]. \quad (33)$$

According to the Karush-Kuhn-Tucker Conditions (KKT conditions), the dual variables are updated using gradient method:

$$\lambda_k^{(j+1)} = \left[ \lambda_k^{(j)} - \theta_k^{(j)} (I_{AM,k-1} - I_{MB,a}^k - I_{MB,b}^k) \right]^+, k = 1, \dots, K, \quad (34)$$

$$\zeta^{(j+1)} = \left[ \zeta^{(j)} - \theta_{K+1}^{(j)} \left( E_A - \sum_{k=0}^{K-1} p_A(R_{AM,k}) \right) \right]^+, \quad (35)$$

$$\xi^{(j+1)} = \left[ \xi^{(j)} - \theta_{K+2}^{(j)} \left( E_M - \sum_a p_M(R_0) - \sum_b p_M(R_{MB,b}) \right) \right]^+, \quad (36)$$

where  $[x]^+$  means  $\max\{x, 0\}$ .  $\theta_k^j, k = 1, \dots, K+2$  are the interaction steps for  $\boldsymbol{\lambda}, \zeta$  and  $\xi$  respectively. The steps should satisfy:

$$\lim_{j \rightarrow \infty} \theta_k^j = 0, \sum_{j=1}^{\infty} \theta_k^j = \infty, k = 1, \dots, K+2. \quad (37)$$

#### Algorithm 1 Design of Communication Power for Given Trajectory

- 1: Initialize the number of time slots  $K$ , the minimum data rate  $R_0$  and the maximum energy consumption  $E_A$  and  $E_M$ . Initialize the relay trajectory  $\{\mathbf{x}, \mathbf{y}, \mathbf{z}\}$  for each time slot  $k$  and the circuit power consumption  $p_c$ ;
- 2: Initialize the maximum iterative number  $J$  and the Lagrange dual variables  $\boldsymbol{\lambda}, \zeta$  and  $\xi$ ;
- 3: Obtain  $\tilde{R}_{MB,k}$  by solving  $\beta(R_{MB,k}) = 0$  with the method of bisection;
- 4: **if**  $\tilde{R}_{MB,k} \leq R_0$  **then**
- 5:      $R_{MB,k} = R_0$ ;
- 6: **else**
- 7:     Record the time number  $k$  for  $\tilde{R}_{MB,k}$  in  $\mathbf{b}$ ;
- 8: **end if**
- 9: **repeat**
- 10:     Find  $\{\mathbf{R}_{AM}, \mathbf{R}_{MB}\} = \arg \max L(\{\mathbf{R}_{AM}, \mathbf{R}_{MB}\}, \{\boldsymbol{\lambda}, \zeta, \xi\})$ ;
- 11:     Update  $\boldsymbol{\lambda}, \zeta$  and  $\xi$  with (34), (35), (36) subject to  $\boldsymbol{\lambda} \geq 0, \zeta \geq 0$  and  $\xi \geq 0$ ;
- 12: **until** The dual variables reach a convergence or  $j = J$
- 13: **Output**  $\mathbf{p}_A$  and  $\mathbf{p}_B$ ;

Algorithm 1 outlines the procedure of finding the optimal solution of (P2'). The time complexity of finding the root of  $\beta(R_{MB,k})$  is  $O(KJ_1)$ , where  $J_1$  is the maximum iterations of the bisection method or the Newton method and  $K$  is the time slot number. If the number of  $\tilde{R}_{M,k} \leq R_0$  is  $A$  in all, and the number of  $\tilde{R}_{M,k} > R_0$  is  $B$ , the time complexity of the Lagrange Multiplier method is  $O(J_3K(BJ_2+K))$ , where  $J_2$  is the maximum iterations to update  $\mathbf{R}_{MB,b}$  using the bisection method, and  $J_3$  is the maximum iterations for Algorithm 1 to converge.  $\mathbf{R}_{MB,a}$  can be determined in the forth and fifth steps in Algorithm 1, thus, are not enrolled in

the iterative updating procedure. So the time complexity of Algorithm 1 is  $O(J_3 K(BJ_2 + K))$ .

#### IV. DESIGNING OF TRAJECTORY FOR GIVEN POWER ALLOCATION

After solving the power allocation problem, we design the trajectory of M. When the power transmitted by A and M are fixed, i.e.,  $\mathbf{p}_A$  and  $\mathbf{p}_M$  are already given. For simplicity, define  $h_{MB,k} = p_{M,k} C_L / (N_0 B)$  and  $h_{AM,k} = p_{A,k} C_L / (N_0 B)$ . To design the trajectory  $\{\mathbf{x}, \mathbf{y}, \mathbf{z}\}$ , we formulate the sub-problem as (P3).

$$\max_{\{\mathbf{x}, \mathbf{y}, \mathbf{z}\}} \sum_{k=1}^K \frac{\log_2 \left( 1 + \frac{h_{MB,k}}{[z_k^2 + (L-x_k)^2 + y_k^2]^{\frac{\alpha_L}{2}}} \right)}{p_{M,k} + p_c} \quad (\text{P3})$$

$$\text{s.t. } z_k \geq \sqrt{z_k^2 + x_k^2 + y_k^2} \sin \eta, \forall k, \quad (38a)$$

$$z_k \geq \sqrt{z_k^2 + (L-x_k)^2 + y_k^2} \sin \eta, \forall k \quad (38b)$$

$$\sum_{i=1}^k \log_2 \left( 1 + \frac{h_{MB,i}}{[z_i^2 + (L-x_i)^2 + y_i^2]^{\frac{\alpha_L}{2}}} \right) \leq \sum_{i=0}^{k-1} \log_2 \left( 1 + \frac{h_{AM,i}}{[z_i^2 + x_i^2 + y_i^2]^{\frac{\alpha_L}{2}}} \right), k = 1, \dots, K, \quad (38c)$$

$$\log_2 \left( 1 + \frac{h_{MB,k}}{[z_k^2 + (L-x_k)^2 + y_k^2]^{\frac{\alpha_L}{2}}} \right) \geq R_0, k = 1, \dots, K \quad (38d)$$

$$(x_k - x_{k-1})^2 + (y_k - y_{k-1})^2 \leq v_0^2 \Delta t^2, k = 1, \dots, K, \quad (38e)$$

$$z_k - z_{k-1} \leq v_c \Delta t, k = 1, \dots, K, \quad (38f)$$

$$(v_{l,k} - v_{l,k-1})^2 + (v_{c,k} - v_{c,k-1})^2 \leq a_{max}^2 \Delta t^2, k = 1, \dots, K-1, \quad (38g)$$

$$H_{min} \leq z_k \leq H_{max}, \forall k, \quad (38h)$$

$$\sum_{k=1}^K \left[ (1+c) \frac{W^{3/2}}{\sqrt{2\rho A}} \sqrt{\sqrt{1 + \frac{v_{l,k}^4}{4v_h^4} - \frac{v_{l,k}^2}{2v_h^2}}} \right. \\ \left. + \sum_{k=1}^K \left[ \frac{\delta \rho S_{blade} v_{tip}^3}{8} \left( 1 + \frac{3v_{l,k}^2}{v_{tip}^2} \right) + \frac{r_d \rho S_{blade} v_{l,k}^3}{2} + W v_{c,k} \right] \right] \\ \leq m_0 c_p \eta_{fuel} / \Delta t. \quad (38i)$$

(P3) is non-convex because of the non-convexity of the objective function and constraints (38a)-(38d) and (38i). To solve (P3), we introduce some slake variables and then use successive convex approximation method.

To deal with the non-convex objective function, we introduce slake variables  $\{\bar{\mathbf{R}}_{MB}\}$ , satisfying

$$\bar{R}_{MB,k} \leq \log_2 \left( 1 + \frac{h_{MB,k}}{[z_k^2 + (L-x_k)^2 + y_k^2]^{\frac{\alpha_L}{2}}} \right), k = 1, \dots, K. \quad (39)$$

Next, we denote  $P_{hover,i} = (1+c) \frac{W^{3/2}}{\sqrt{2\rho A}}$ ,  $P_{hover,b} = \frac{\delta \rho S_{blade} v_{tip}^3}{8}$  and  $\tilde{P}_p = \frac{r_d \rho S_{blade}}{2}$  for concise representation

in the subsequent analysis. To deal with the non-convex constraint (38i), we use the equality  $\sqrt{1+x} - \sqrt{x} = 1/(\sqrt{1+x} + \sqrt{x})$  to rewrite the first term of (38i) in the following form,

$$(1+c) \frac{W^{3/2}}{\sqrt{2\rho A}} \sqrt{\sqrt{1 + \frac{v_{l,k}^4}{4v_h^4} - \frac{v_{l,k}^2}{2v_h^2}}} = \frac{P_{hover,i}}{\sqrt{\sqrt{1 + \frac{v_{l,k}^4}{4v_h^4} + \frac{v_{l,k}^2}{2v_h^2}}}}. \quad (40)$$

Then we rewrite (38i) as constraints (41)-(45) by adding slake variables  $\mathbf{m}, \mathbf{n}, \mathbf{p}$ , and  $\mathbf{q}$ , denoting sets of  $m_k, n_k, p_k, q_k, k = 1, \dots, K$  respectively.

$$\sum_{k=1}^K \left[ P_{hover,i} m_k + P_{hover,b} \left( 1 + \frac{3v_{l,k}^2}{v_{tip}^2} \right) + \tilde{P}_p v_{l,k}^3 + W v_{c,k} \right] \\ \leq m_0 c_p \eta_{fuel} / \Delta t, \quad (41)$$

$$m_k \geq \frac{1}{n_k}, \quad (42)$$

$$n_k^2 \leq \sqrt{p_k} + \frac{q_k}{2v_h^2}, \quad (43)$$

$$p_k \leq 1 + \frac{q_k^2}{4v_h^4}, \quad (44)$$

$$q_k \leq \frac{(x_k - x_{k-1})^2 + (y_k - y_{k-1})^2}{\Delta t^2}. \quad (45)$$

Then (P3) can be rewritten as (P3')

$$\max_{\mathbf{x}, \mathbf{y}, \mathbf{z}, \bar{\mathbf{R}}_{MB}, \mathbf{m}, \mathbf{n}, \mathbf{p}, \mathbf{q}} \sum_{k=1}^K \frac{\bar{R}_{MB,k}}{p_{M,k} + p_c} \quad (\text{P3}')$$

$$\text{s.t. (38a), (38b), (38e)-(38h), (39), (41)-(45),}$$

$$\sum_{i=1}^k \bar{R}_{MB,i} \leq \sum_{i=0}^{k-1} \log_2 \left( 1 + \frac{h_{AM,i}}{[z_i^2 + x_i^2 + y_i^2]^{\frac{\alpha_L}{2}}} \right), \\ k = 1, \dots, K, \quad (46a)$$

$$\bar{R}_{MB,k} \geq R_0, k = 1, \dots, K. \quad (46b)$$

(41)-(45) form a tight lower bound of (38i). If (38i) is satisfied with equality, constraints (41)-(45) are always satisfied with equality. Here is a brief explanation using reduction to absurdity. As an assumption, for example, (45) is not active, which means  $q_k < \frac{(x_k - x_{k-1})^2 + (y_k - y_{k-1})^2}{\Delta t^2}$ . One can always increase  $q_k$  to make (45) an equality. Analogically,  $p_k, n_k$  can be increased in (44) and (43) as well, then one can always reduce  $m_k$  to make (42) satisfied with equality. Then the left side of (41) becomes smaller. This leads to a contradiction with the premise that (38i) is an active constraint. So (41)-(45) form a tight lower bound of (38i).

The non-convex constraints for (P3') are (38a), (38b), (39), (44), (45) and (46a). They are all in the form of a difference of two convex functions. The problem can be solved sub-optimally with successive convex approximation [1].

After iteration  $l$  of the successive convex approximation method, we update the positions of the UAV  $\{\mathbf{x}, \mathbf{y}, \mathbf{z}\}$  and the slake variables  $\mathbf{q}$  by

$$[\mathbf{x}^l, \mathbf{y}^l, \mathbf{z}^l] = [\mathbf{x}^{l-1}, \mathbf{y}^{l-1}, \mathbf{z}^{l-1}] + [\Delta \mathbf{x}^l, \Delta \mathbf{y}^l, \Delta \mathbf{z}^l], \quad (47)$$

$$\mathbf{q}^l = \mathbf{q}^{l-1} + \Delta \mathbf{q}^l. \quad (48)$$

For simplicity, we use  $l_{AM,k}^{l-1}$  and  $l_{BM,k}^{l-1}$  to represent the distance of A to M and the distance of M to B after the  $(l-1)$ th iteration. And we use  $\Delta_{AM,k}^l$  and  $\Delta_{MB,k}^l$  to imply the increment of the square of distances after the  $l$ th iteration, i.e.,

$$l_{AM,k}^{l-1} = \left[ (x_k^{l-1})^2 + (y_k^{l-1})^2 + (z_k^{l-1})^2 \right]^{\frac{1}{2}}, \quad (49)$$

$$l_{BM,k}^{l-1} = \left[ (L_0 - x_k^{l-1})^2 + (y_k^{l-1})^2 + (z_k^{l-1})^2 \right]^{\frac{1}{2}}, \quad (50)$$

$$\Delta_{AM,k}^l = (\Delta x_k^l)^2 + (\Delta y_k^l)^2 + (\Delta z_k^l)^2 + 2x_k^{l-1} \Delta x_k^l + 2y_k^{l-1} \Delta y_k^l + 2z_k^{l-1} \Delta z_k^l, \quad (51)$$

$$\Delta_{MB,k}^l = (\Delta x_k^l)^2 + (\Delta y_k^l)^2 + (\Delta z_k^l)^2 - 2(L_0 - x_k^{l-1}) \Delta x_k^l + 2y_k^{l-1} \Delta y_k^l + 2z_k^{l-1} \Delta z_k^l. \quad (52)$$

First, to make (38a) and (38b) convex, using the inequality  $(A+x)^{\frac{1}{2}} \leq A^{\frac{1}{2}} + \frac{1}{2}A^{-\frac{1}{2}}x$ ,  $x \geq 0$ , we obtain the upper bound for the right side of (38a) by letting  $A = (l_{AM,k}^{l-1})^2$  and  $x = \Delta_{AM,k}^l$ , and obtain the convex constraints

$$z_k^{l-1} + \Delta z_k^l \geq \sin \eta \left[ l_{AM,k}^{l-1} + \frac{1}{2} (l_{AM,k}^{l-1})^{-1} (\Delta_{AM,k}^l) \right], \forall k, \quad (53)$$

Similarly, we slake (38b) to convex constraints

$$z_k^{l-1} + \Delta z_k^l \geq \sin \eta \left[ l_{MB,k}^{l-1} + \frac{1}{2} (l_{MB,k}^{l-1})^{-1} (\Delta_{MB,k}^l) \right], \forall k. \quad (54)$$

Since  $\alpha_L/2 > 1$ ,  $\log_2 \left( 1 + \frac{A}{x^{\frac{\alpha_L}{2}}} \right)$  is convex for  $x > 0$  because its second-order derivative is positive. Its first-order Taylor expansion at  $x_0$  can be used as a lower bound:

$$\log_2 \left( 1 + \frac{A}{x^{\frac{\alpha_L}{2}}} \right) \geq \log_2 \left( 1 + \frac{A}{x_0^{\frac{\alpha_L}{2}}} \right) + \frac{-\frac{\alpha_L}{2} A}{\ln 2 \cdot x_0 (x_0^{\frac{\alpha_L}{2}} + A)} (x - x_0). \quad (55)$$

Note that the symbols  $A$ ,  $x$  and  $x_0$  are used temporarily in (55) for succinctness. They are irrelevant with the ones appearing in our system model. In (39), by letting  $A = h_{MB,k}$ ,  $x = (l_{MB}^{l-1})^2 + \Delta_{MB}^l$ , and  $x_0 = (l_{MB}^{l-1})^2$ , we have:

$$\bar{R}_{MB,k} \leq R_{MB,k}^{l-1} + D_{MB,k}^l \Delta_{MB,k}^l, k = 1, \dots, K, \quad (56)$$

where  $D_{MB,k}^l = \frac{-\frac{\alpha_L}{2} h_{MB,k}}{\ln 2 \cdot (l_{MB,k}^{l-1})^2 [(l_{MB,k}^{l-1})^{\alpha_L} + h_{MB,k}]}$ .

Similarly, we transmit (46a) as:

$$\sum_{i=1}^k \bar{R}_{MB,i} \leq \sum_{i=0}^{k-1} \left( R_{AM,k}^{l-1} + D_{AM,k}^l \Delta_{AM,k}^l \right), k = 1, \dots, K \quad (57)$$

where  $D_{AM,k}^l = \frac{-\frac{\alpha_L}{2} h_{AM,k}}{\ln 2 \cdot (l_{AM,k}^{l-1})^2 [(l_{AM,k}^{l-1})^{\alpha_L} + h_{AM,k}]}$ .

Next, referring to the inequality function that  $x^2 \geq x_0^2 + 2x_0(x - x_0)$ , We transfer (44) to convex constraints by replacing the right side of the inequality function with their lower bound as

$$p_k \leq 1 + \frac{(q_k^{l-1})^2 + 2q_k^{l-1} \Delta q_k^l}{4v_h^4}, \forall k. \quad (58)$$

And (45) can be transferred to convex constraints

$$q_k^{l-1} + \Delta q_k^l \leq \left( v_{x,k}^{l-1} \right)^2 + 2v_{x,k}^{l-1} \frac{\Delta x_k^l - \Delta x_{k-1}^l}{\Delta t} + \left( v_{y,k}^{l-1} \right)^2 + 2v_{y,k}^{l-1} \frac{\Delta y_k^l - \Delta y_{k-1}^l}{\Delta t}, \forall k, \quad (59)$$

where  $v_{x,k}^{l-1} = (x_k^{l-1} - x_{k-1}^{l-1})/\Delta t$ ,  $v_{y,k}^{l-1} = (y_k^{l-1} - y_{k-1}^{l-1})/\Delta t$ .

Then, we can find a suboptimal solution for the non-convex function (P3) by solving (P4).

$$\begin{aligned} \max_{\Delta \mathbf{x}, \Delta \mathbf{y}, \Delta \mathbf{z}, \bar{\mathbf{R}}_{MB}, \mathbf{m}, \mathbf{n}, \mathbf{p}, \Delta \mathbf{q}} \quad & \sum_{k=1}^K \frac{\bar{R}_{MB,k}}{p_{M,k} + p_c} \\ \text{s.t.} \quad & (53), (54), (56)-(59), \\ & (38e)-(38h), (41)-(43), (46b). \end{aligned} \quad (P4)$$

(P4) is a convex problem, because the objective function is concave and all the constraints are convex. We can solve it using the CVX toolbox in MATLAB. By updating the solutions iteratively, the solution of (P4) converges to a suboptimal solution of (P3). The successive convex approximation method to solve (P3) is summarized in Algorithm 2. The convergence of the successive convex approximation method can be proved similarly as in [38]. Since CVX toolbox uses the interior point method, the complexity of solving problem (P4) is  $O(K^{3.5} \log(1/\epsilon))$  [42], where  $\epsilon$  is the convergence tolerance. Then the complexity of Algorithm 2 is  $O(J_4(K^{3.5} \log(1/\epsilon)))$ , where  $J_4$  is the iteration time of the outloop of Algorithm 2.

---

#### Algorithm 2 Suboptimal Trajectory Solution for Fixed Power Allocation

---

- 1: Initialize the UAV's trajectory  $\{\mathbf{x}^0, \mathbf{y}^0, \mathbf{z}^0\}$ ,  $\mathbf{q}^0$ . Set the maximum iteration  $l_m$ . Let  $l = 1$ ;
  - 2: **repeat**
  - 3: Use  $\{\mathbf{x}^{l-1}, \mathbf{y}^{l-1}, \mathbf{z}^{l-1}\}$ ,  $\mathbf{q}^{l-1}$  in (P4) and obtain the converged solutions  $\Delta \mathbf{x}, \Delta \mathbf{y}, \Delta \mathbf{z}, \bar{\mathbf{R}}_{MB}, \mathbf{m}, \mathbf{n}, \mathbf{p}, \Delta \mathbf{q}$ ;
  - 4: Update  $\{\mathbf{x}^l, \mathbf{y}^l, \mathbf{z}^l\}$ ,  $\mathbf{q}^l$  by (47) and (48).
  - 5: Update the iteration time  $l = l + 1$ .
  - 6: **until** The value of the objective function reaches a convergence or  $l = l_m$
- 

## V. JOINT POWER AND TRAJECTORY DESIGN

In this section, based on the results in Sections III and IV, a jointly iterative algorithm is proposed in Algorithm 3. Algorithm 3 works by solving the two convex problems (P2') and (P4) iteratively. For initialized trajectory, Algorithm 1 finds the power allocation scheme for all the time slots. When the power allocation scheme is given, Algorithm 2 works to design the trajectory of the relay. The convergence of Algorithm 3 needs  $J_5$  iteration. Based on the complexity of Algorithms 1 and 2, the complexity of Algorithm 3 is  $O((J_3 K (BJ_2 + K) + J_4 K^{3.5} \log(1/\epsilon)) J_5)$ .

Then we prove the convergence of Algorithm 3. Denote the objective function of (P1) after the  $t$ th iteration

as  $EE(\{\mathbf{p}_{AM}^t, \mathbf{p}_{MB}^t\}, \{\mathbf{x}^t, \mathbf{y}^t, \mathbf{z}^t\})$ . Since Algorithm 1 converges to the optimal solution of (P2), and Algorithm 2 converges to the suboptimal solution of (P3), we have

$$EE(\{\mathbf{p}_{AM}^{t+1}, \mathbf{p}_{MB}^{t+1}\}, \{\mathbf{x}^t, \mathbf{y}^t, \mathbf{z}^t\}) \geq EE(\{\mathbf{p}_{AM}^t, \mathbf{p}_{MB}^t\}, \{\mathbf{x}^t, \mathbf{y}^t, \mathbf{z}^t\}). \quad (61)$$

Also, after running Algorithm 2, we have

$$EE(\{\mathbf{p}_{AM}^{t+1}, \mathbf{p}_{MB}^{t+1}\}, \{\mathbf{x}^{t+1}, \mathbf{y}^{t+1}, \mathbf{z}^{t+1}\}) \geq EE(\{\mathbf{p}_{AM}^{t+1}, \mathbf{p}_{MB}^{t+1}\}, \{\mathbf{x}^t, \mathbf{y}^t, \mathbf{z}^t\}). \quad (62)$$

Consequently,

$$EE(\{\mathbf{p}_{AM}^{t+1}, \mathbf{p}_{MB}^{t+1}\}, \{\mathbf{x}^{t+1}, \mathbf{y}^{t+1}, \mathbf{z}^{t+1}\}) \geq EE(\{\mathbf{p}_{AM}^t, \mathbf{p}_{MB}^t\}, \{\mathbf{x}^t, \mathbf{y}^t, \mathbf{z}^t\}). \quad (63)$$

Thus  $EE$  is non-decreasing with the iterations. Since  $EE$  will be not larger than its optimal value, Algorithm 3 converges to a global or local solution for (P1).

### Algorithm 3 Jointly Communication Power and Relay Trajectory Design

- 1: Initialize the UAV's trajectory  $\{\mathbf{x}, \mathbf{y}, \mathbf{z}\}$ . Set the minimum data rate  $R_0$  and the maximum electric energy consumptions  $E_A$  and  $E_M$ , the maximum fuel consumption  $m_0$ . Set the channel coefficient  $C_L$  and  $\alpha_L$ , the noise power spectral  $N_0$ , the bandwidth  $B$ , the circuit power  $p_c$ , the maximum speed  $v_0, v_c$  and the height constraints  $H_{min}, H_{max}$ . Initiate the iteration  $t = 0$ , set the convergence tolerance  $\epsilon$ .
- 2: **repeat**
- 3: For fixed trajectory, use Algorithm 1 to decide the power allocation for A and M;
- 4: Use the power allocation results given in step 3 to solve the trajectory of M using Algorithm 2;
- 5: **until** The result reaches a convergence or the iteration time reaches the upper limit.

## VI. NUMERICAL RESULTS AND DISCUSSION

In this section, numerical results are shown to illustrate the performance of the power allocation and trajectory design schemes. The parameters of the channel models are listed in Table I [38] [32]. The parameters of the UAV movement and mechanical power are listed in Table II. Without additional illustration, the numerical results are solved based on Table I and Table II.

TABLE I  
CHANNEL MODEL PARAMETERS.

Notation	Meaning	Value
$L_0$	Distance between A and B	2000m
$T$	Total time	100s
$\alpha_0$	Parameter in (4) for suburban	4.88
$\beta_0$	Parameter in (4) for suburban	0.429
$B$	Bandwidth	20MHz
$N_0$	Noise spectrum density	-169dBm/Hz
$F$	Frequency	5GHz
$C_{LoS}$	Path loss of parameters in LoS	-46dB
$C_{NLoS}$	Path loss of parameters in NLoS	-53.4dB
$\alpha_L$	Path loss exponent in LoS	2
$\alpha_N$	Path loss exponent in NLoS	2.7
$\eta$	Elevation angle constraint	20°
$R_0$	Minimum data rate constraint for B	12Mbps

TABLE II  
CHANNEL MODEL PARAMETERS.

Notation	Meaning	Value
$c$	Incremental correction factor in (11)	0.1
$W$	UAV weight	$20 \times 9.8N$
$\rho$	Air density	$1.225kg/m^3$
$v_h$	Induced velocity in hovering	5.0463m/s
$\delta$	Profile drag coefficient	0.012
$S_{blade}$	Total blade area	$0.2m^2$
$r_d$	Fuselage drag ratio	0.6
$v_{tip}$	Speed of rotor blade tip	250m/s
$c_p$	Heat of combustion of fuel	43.5MJ/kg
$\eta_{fuel}$	Average thermodynamic efficiency of the gas turbine	0.45
$v_0$	Maximum horizontal speed	30m/s
$v_c$	Maximum vertical speed	6m/s
$a_{max}$	Maximum acceleration	$2m/s^2$
$H_{max}$	Highest height constraint	1000m
$H_{min}$	Lowest height constraint	200m

We show the convergence of Algorithm 3 and the influence of the length of time slots to the solutions. The UAV starts from above the source node and ends above the destination node. The maximum communication power is less than 13dBm for A and M. The fuel consumption is less than 0.035kg. Other parameters are set according to Table I and Table II. As shown in Fig. 3, the average energy efficiency decreases when the intervals are larger. The results seem to contradict with intuition, but they make sense. There are two ways in which  $\Delta t$  influences the results. Firstly, the UAV is assumed to fly at constant speeds during each time slot. When  $\Delta t$  increases, the UAV changes its speed for less number of times during the whole mission. This restricts the movement of the UAV. Another influence of  $\Delta t$  is the distance approximation error to solve the data rate. There are  $K$  time slots and  $K + 1$  nodes, including  $K - 1$  nodes between the time slots and 2 nodes on the two sides of the total time  $T$ . As we assumed in II-D, the positions of the UAV at the beginning of each time slot are used to compute  $l_{AM}$  and  $R_{AM}$  during the time slot, and the positions of the UAV at the end of the time slot are used to compute  $l_{MB}$  and  $R_{MB}$  during the time slot. When the UAV moves from above A to above B, the approximated path loss is smaller than what it should be. This makes the approximated  $R_{AM}$  and  $R_{MB}$  higher than the actual  $R_{AM}$  and  $R_{MB}$  during the time slot, and thus increase the energy efficiency.

In the related work, we could find that time slots were chosen to be several seconds, for example 0.5s, 1s and 2.5s [38], [43], [44]. Since the time slot influences the approximation of distance of the UAV and ground users, thus influencing the data rates. We have derived a bound for the approximation error of data rates related to the length of time slots. Referring to the inequality (55), the bound for the absolute estimation error of data rate can be derived as follows.

During each time slot, the maximum change of distance  $l$  caused by the UAV's movement during the time slot is defined as  $\Delta l$ ,  $\Delta l \leq v_{max} \Delta t$ . Denote  $\theta$  as the angle between the speed and  $l$ ,  $0 \leq \theta \leq \pi$ . For simplicity, let  $p$  represent the power transmitted from the transmitter A or M. Then we define the absolute estimation error of data rate as

$$e = |\log_2 \left( 1 + \frac{ptC_{LoS}}{l^\alpha N_0 B} \right) - \log_2 \left( 1 + \frac{ptC_{LoS}}{(l + \Delta l \cos \theta)^\alpha N_0 B} \right)|. \quad (64)$$

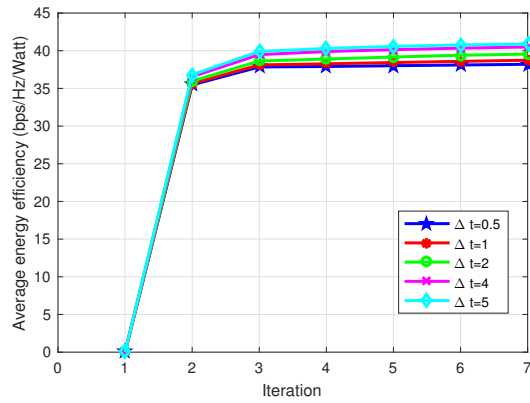


Fig. 3. Convergence of Algorithm 3 and influence of  $\Delta t$ .

Without loss of generality, suppose  $\Delta l \cos \theta \geq 0$ , then we have

$$e = \log_2 \left( 1 + \frac{p_t C_{LoS}}{l^\alpha N_0 B} \right) - \log_2 \left( 1 + \frac{p_t C_{LoS}}{(l + \Delta l \cos \theta)^\alpha N_0 B} \right). \quad (65)$$

Referring to the inequality (55), since  $\alpha > 1$ , we have

$$\begin{aligned} & \log_2 \left( 1 + \frac{p_t C_{LoS}}{(l + \Delta l \cos \theta)^\alpha N_0 B} \right) \\ & \geq \log_2 \left( 1 + \frac{p_t C_{LoS}}{l^\alpha N_0 B} \right) - \frac{\alpha \frac{p_t C_{LoS}}{N_0 B}}{\ln 2 \cdot l (l^\alpha + p_t C_{LoS}/N_0 B)} \cdot \Delta l \cos \theta. \end{aligned} \quad (66)$$

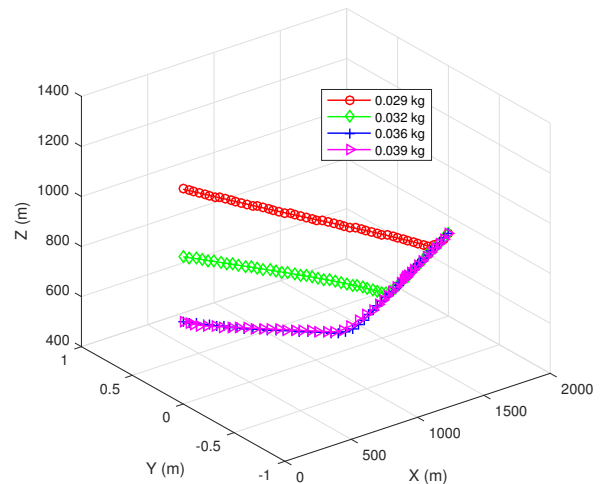
Thus the estimation error is bounded as

$$e \leq \frac{\alpha \frac{p_t C_{LoS}}{N_0 B}}{\ln 2 \cdot l (l^\alpha + p_t C_{LoS}/N_0 B)} \cdot v_{max} \Delta t. \quad (67)$$

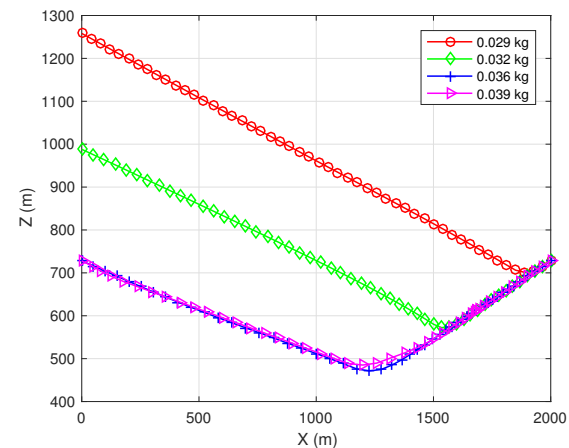
Thus for certain channel condition, the approximation error of data rates are related to the length of time slots  $\Delta t$ , the maximum speed of the UAV,  $v_{max}$ , and the geometry distance of the UAV to ground nodes,  $l$ .

To show the performance of the proposed algorithm, we use the global optimal tool MultiStart in Matlab as a comparison. MultiStart solves non-convex problem by searching from a large number of starting points and choose the best result, to increase the possibility of finding the global optimal result. It can be seen that the proposed sub-optimal algorithm can achieve close results compared to MultiStart in Fig. 6. The line with diamond markers shows the simulation results computed according to (7). The LoS channel has Rician fading, with Rician factor  $k = 10$ , and the NLoS channel has Rayleigh fading. It shows that (9) approximates the channel well.

To see the influence of the fuel weight, we consider the UAV to start from above the source node and end above the destination node. The average communication power consumption is 16dBm. The fuel supply is set to range from 0.029kg to 0.039 kg. The time slot length is 2s. The UAV's altitude is constrained to be lower than 1500m. Fig. 4(a) shows the 3D trajectory of the UAV. Fig. 4(b) shows the vertical plane of the trajectory at  $y = 0m$ . In Fig. 5,  $v_t$  is the total velocity, which is the vector sum of vertical velocity and the horizontal velocity.  $v_l$  means the speed on the level plane.  $v_c$  is the vertical speed. When the fuel supplied is set to be too short, i.e., 0.029kg and 0.032kg, the UAV takes more time to decrease to save



(a) 3D trajectory



(b) Trajectory on vertical plane

Fig. 4. Trajectory of the UAV.

fuel, even when the channel condition is worse. This happens because we do not consider the energy consumption before the communication starts. The UAV cannot travel with the highest level speed or hover because it would be more energy-consuming [37]. When more fuel is available, the UAV is able to decrease and increase its altitude, to get closer to the nodes A and B. Fig. 5 also shows that the UAV is also able to travel with higher speed or hover for longer time. Fig. 6 shows that the energy efficiency increases and when the fuel supply increases. Then it stays at a constant value because the fuel is enough for the UAV to obtain good trajectory and speeds.

Fig. 7 shows the influence of available communication power. The maximum fuel consumption is 0.035kg. We consider three benchmark schemes. Benchmark scheme 1 is fixing the UAV above (800m, 0m) and designing the height of the UAV. Benchmark scheme 2 is fixing the UAV above the midpoint of A and B, which is (1000m, 0m), and benchmark scheme 3 is fixing the UAV above (1200m, 0m). Proposed scheme 1 is fixing the UAV's starting point and ending point

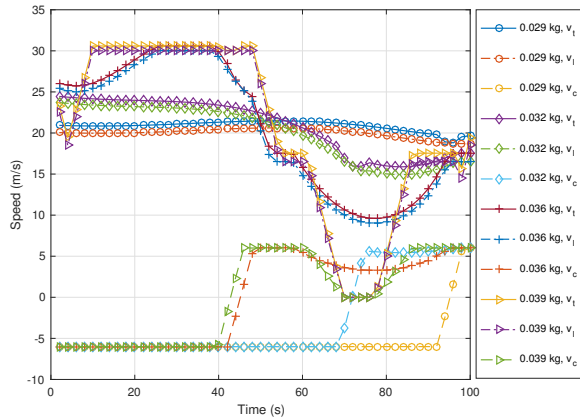


Fig. 5. Speed versus time

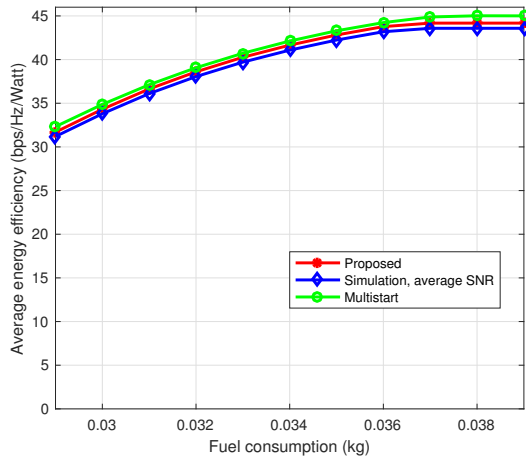


Fig. 6. Influence of the fuel weight.

above the source node and destination node respectively. Proposed scheme 2 is not fixing the UAV's starting node and ending node. As shown in Fig. 7, proposed scheme 2 achieves higher energy efficiency than the benchmarks and proposed scheme 1. When the average communication consumption is less than around 12.8dBm, both the two proposed schemes 1 and 2 achieve higher energy efficiency than the three benchmarks. The results implies that with fewer communication power, the average energy efficiency benefits more from the UAV's movement.

Further, it can be seen from Fig. 7 that before the energy efficiency reaches a constant value, the slopes of the three lines of baseline schemes 1, 2, and 3 are different. To discuss this, we first prove that when the UAV's position is fixed, the optimal communication energy for all the time slots are the equal. This is because the UAV stays stationary and thus the channel coefficients for all time slots are stable. As proved in Property 1, the objective function of (P2') is concave. Thus according to Jensen's inequality,

$$f\left(\frac{x_1 + \dots + x_N}{N}\right) \geq \frac{f(x_1) + \dots + f(x_N)}{N}, \quad (68)$$

the maximum  $\frac{f(x_1) + \dots + f(x_N)}{N}$  can be established when  $x_1 = \dots = x_N$ . Using contradiction, suppose there exist two time slots  $k_1$  and  $k_2$ , the optimal data rates satisfying  $R_{MB,k_1} < R_{MB,k_2}$  and  $R_{AM,k_1} < R_{AM,k_2}$ . Then one can always make  $R_{MB,k_1} = R_{MB,k_2} = \frac{R_{MB,k_1} + R_{MB,k_2}}{2}$  and  $R_{AM,k_1} = R_{AM,k_2} = \frac{R_{AM,k_1} + R_{AM,k_2}}{2}$  without violating the constraints, and making the objective function larger. Thus the optimal solution should be equal data rates  $R_{AM}$  and  $R_{MB}$  for all time slots, and consequently, equal  $p_A$  and  $p_M$  for all time slots. The results in Fig. 8 and Fig. 9 are consistent with the analysis.

Then we explain the line slopes. Now that the power and data rate in all time slots are equal, we use footmarks 1, 2, and 3 to represent baseline schemes 1, 2, and 3, for example,  $R_{AM,1}$  is the data rate at any time slots of baseline scheme 1. The channel condition of A to M is better than that of M to B in baseline scheme 1. Achieving the same data rate  $R_{AM,1} = R_{MB,1}$  requires less power from A than from M. Thus with equal power supply for A and M, the information causality constraints can be always satisfied. The energy efficiency depends on the power from M.

$$EE_{scheme1} = \frac{\log_2\left(1 + p_{M,1} \frac{C_{LoS}}{l_{MB,1}^\alpha N_0 B}\right)}{p_{M,1} + p_c}. \quad (69)$$

As for baseline scheme 3, the channel of M to B is better. The information causality constraints (15b) is active. Thus the bottleneck for the data rate at M is the received information from A. We have

$$\begin{aligned} R_{MB,3} &= \log_2\left(1 + p_{M,3} \frac{C_{LoS}}{l_{MB,3}^\alpha N_0 B}\right) \\ &= \log_2\left(1 + p_{A,3} \frac{C_{LoS}}{l_{AM,3}^\alpha N_0 B}\right). \end{aligned} \quad (70)$$

So the relationship of  $p_{A,3}$  and  $p_{M,3}$  is

$$p_{M,3} = \frac{p_{A,3} l_{MB}^\alpha}{l_{AM}^\alpha}. \quad (71)$$

Bringing (71) into (72):

$$EE_{scheme3} = \frac{\log_2\left(1 + p_{M,3} \frac{C_{LoS}}{l_{MB,3}^\alpha N_0 B}\right)}{p_{M,3} + p_c}, \quad (72)$$

we have

$$EE_{scheme3} = \frac{\log_2\left(1 + \frac{p_{A,3} C_{LoS}}{l_{AM,3}^\alpha N_0 B}\right)}{\frac{p_{A,3} l_{MB,3}^\alpha}{l_{AM,3}^\alpha} + p_c}. \quad (73)$$

As for baseline scheme 2, it can be regarded as a special case of baseline schemes 1 or 3 with  $l_{MB} = l_{AM}$ , thus we have

$$\begin{aligned} EE_{scheme2} &= \frac{\log_2\left(1 + p_{A,2} \frac{C_{LoS}}{l_{AM,2}^\alpha N_0 B}\right)}{p_{A,2} + p_c} \\ &= \frac{\log_2\left(1 + p_{M,2} \frac{C_{LoS}}{l_{MB,2}^\alpha N_0 B}\right)}{p_{M,2} + p_c}. \end{aligned} \quad (74)$$

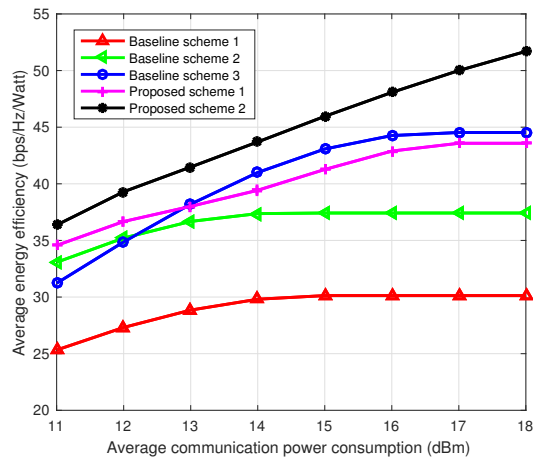


Fig. 7. Influence of communication power constraints.

When the communication power constraints for A and M are set to be equal, denote  $E_A = E_M = E$ . If A or M consumes all the available power, it will be

$$p_{M,1} = E/N, p_{A,3} = E/N. \quad (75)$$

Thus (69) can be derived as

$$EE_{scheme1} = \frac{\log_2 \left( 1 + E/N \frac{C_{LoS}}{I_{MB,1}^\alpha N_0 B} \right)}{E/N + p_c}. \quad (76)$$

(73) can be derived as

$$EE_{scheme3} = \frac{\log_2 \left( 1 + E/N \frac{C_{LoS}}{I_{AM,3}^\alpha N_0 B} \right)}{\frac{E I_{MB,3}^\alpha}{N I_{AM,3}^\alpha} + p_c}. \quad (77)$$

(74) can be derived as

$$EE_{scheme2} = \frac{\log_2 \left( 1 + E/N \frac{C_{LoS}}{I_{MB,2}^\alpha N_0 B} \right)}{E/N + p_c}. \quad (78)$$

The numerators of the equations (76), (77) and (78) are similar. But the denominator of (77) has an extra  $\frac{I_{MB}^\alpha}{I_{AM}^\alpha}$ . Since for scheme 3,  $\frac{I_{MB}^\alpha}{I_{AM}^\alpha}$  is smaller than 1, the energy efficiency grows faster when the abscissa axis  $E$  increases. This explains the different slopes of baseline schemes 1, 2 and 3 in Fig. 7.

Note that equations (76), (77) and (78) only represent the situation when A or M communicate with all the available energy. Fig. 7 also shows that when the communication power gets larger, the energy efficiency in schemes 1, 2 and 3 do not keep increasing. According to Lemma 1, for given trajectory, the energy efficiency increases first and then decreases when  $R_{MB}$  increases. So is not always the most energy-efficient choice to communicate with as much power as possible. So, when the communication energy supply gets larger, the optimal energy efficiency would increase and then stays constant.

Fig. 8 shows the communication power allocation versus time. We set the average communication power constraint as 14dBm. Fig. 8 (a) shows the power transmitted by A. Fig. 8 (b)

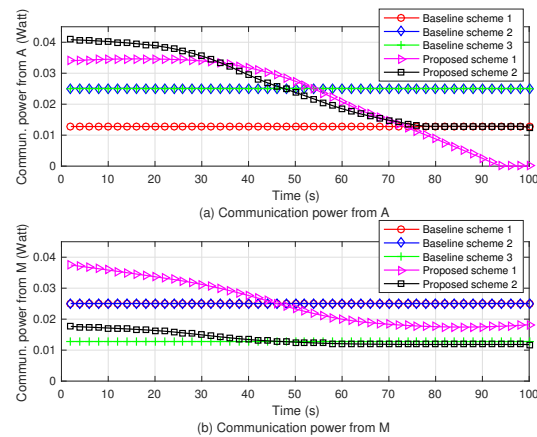


Fig. 8. Communication power from the source node and the UAV.

presents the power transmitted by M. For benchmark scheme 1, the communication power from A is lower than them with benchmark schemes 2 and 3. For benchmark schemes 2 and 3, the communication power from A are coincide, both using the highest achievable power. For proposed schemes 1 and 2, A transmits data to M with more power at the beginning, then it decreases the power transmission when the M gets further from A. In Fig. 8 (b), M communicates with the maximum achievable power to B for benchmark schemes 1 and 2. As for benchmark scheme 3, since the UAV is far from A, the bottleneck is the received data from the source node. Although M has surplus communication power, it dose not have data to transmit. In proposed schemes 1 and 2, the UAV communicates with more power at the beginning because it needs to satisfy the demand of minimum data rate for B. When the UAV moves near the destination node, it communicates with less power. Fig. 9 (a) shows the received data rate at M. Fig. 9 (b) presents the data rate at B. The data rate in benchmark schemes 1 and 3 are the same. The positions of benchmark schemes 1 and 3 are symmetrical about the midpoint. For benchmark scheme 1, the bottleneck is the power from M to B, while for benchmark scheme 3 the bottleneck is the power from A to B. Corresponding to Fig. 8 and Fig. 9, the trajectory and placement of the UAV for benchmark schemes and proposed schemes are shown in Fig. 10.

In Fig. 11, the influence of the constraint  $R_0$  is shown. We set the fuel supply as 0.036kg. The maximum communication energy for A and M are both 13 dBm. With the required data rate of the destination node increasing, the energy efficiencies of benchmark schemes 1-3 do not change. Because for benchmark schemes 1-3, the source node or the UAV always communicates with constant communication power, which can also be seen in Fig.8 and Fig. 9. As for proposed scheme 1, when the required data rate of B increases, the average energy efficiency decreases. This is because to guarantee the required data rate, the UAV needs to consume more energy when the channel condition is not well. For proposed scheme 2, with the required data rate increasing, the average energy efficiency decreases with small scope. The UAV is able adjust its trajectory as well as starting and ending positions and fits

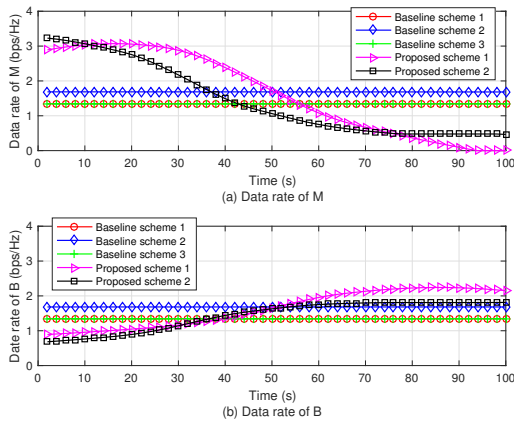
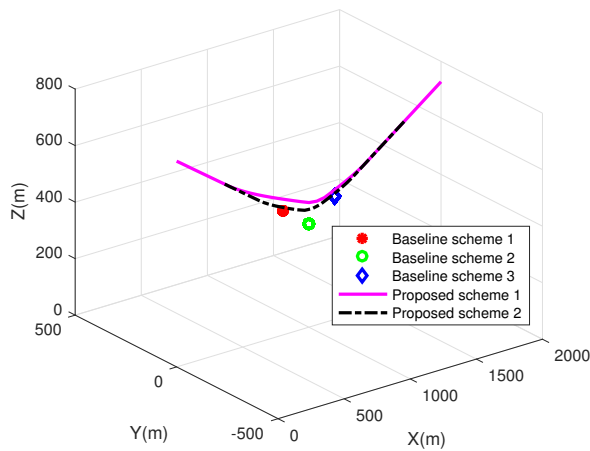
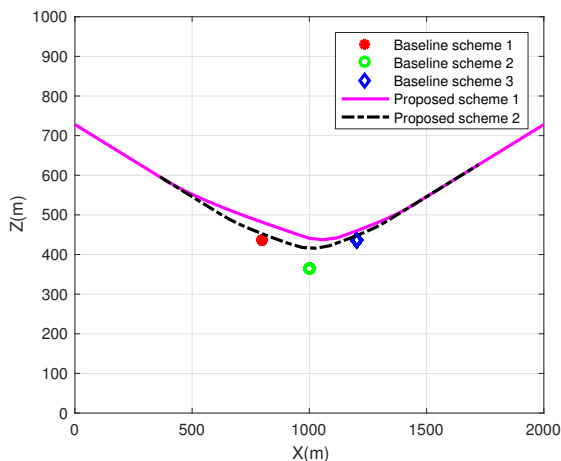


Fig. 9. Data rates from the source node and the UAV.



(a) 3D trajectory and placement of the UAV.



(b) Vertical plane of the UAV trajectory and placement.

Fig. 10. Trajectory of the UAV.

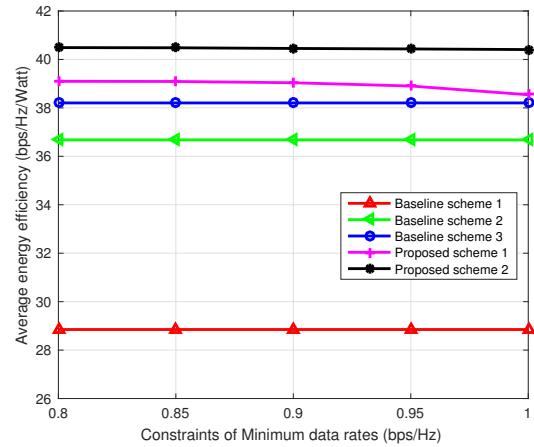


Fig. 11. Influence of  $R_0$ .

the requirement better.

## VII. CONCLUSION

In this paper, we investigated the power allocation and UAV's trajectory to maximize the energy efficiency of a fuel-powered UAV relay under the constraints of communication power and fuel consumption. The minimum data rate for the destination node was guaranteed. We solved the non-convex optimization problem by considering the power allocation and trajectory of the UAV separately. The power allocation sub-problem was transferred to an equivalent convex problem and solved by Lagrange Multiplier Method, which was summarized in Algorithm 1. A sub-optimal trajectory design solution was proposed using successive convex approximation method, which was summarized in Algorithm 2. On the basis of the two algorithms, the problem was solved iteratively according to Algorithm 3. Numerical results show the convergence of the proposed algorithm, and the influences of time slots, fuel supply, communication power, and required data rates. The approximation error of data rate was derived to represent the influence of time slots. The subsequent work can be extended to designing the height and elevation angle of the UAV in more complicated channel conditions and considering more ground users or UAVs with interferences.

## APPENDIX A

### PROOF OF QUASI-CONCAVITY OF $E(R_{MB,k})$

It can be proved that  $E(R_{MB,k})$  is quasi-concave if and only if it has a strictly convex  $\alpha$ -sublevel set, which is defined by

$$S_\alpha = \{R_{M,k} > 0 \mid E(R_{MB,k}) \geq \alpha\}. \quad (79)$$

When  $\alpha \leq 0$ ,  $S_\alpha$  is a strictly convex set because of the non-negativity of  $E(R_{MB,k})$ .

When  $\alpha > 0$ ,  $S_\alpha$  is rewritten as

$$S_\alpha = \{R_{MB,k} > 0 \mid p_M(R_{MB,k})\alpha + p_C\alpha - R_{MB,k} \leq 0\}. \quad (80)$$

Since  $p_M(R_{MB,k})$  is strictly convex for  $R_{MB,k}$ ,  $S_\alpha$  is a strictly convex set as well.

As a result,  $E(R_{MB,k})$  is proved to be strictly quasi-concave.

## APPENDIX B

### PROOF OF LEMMA 1

From the definition of  $\beta(R_{MB,k})$ , we have

$$\begin{aligned} \beta(R_{MB,k}) &= p_c + p_M(R_{MB,k}) - R_{MB,k} \cdot p'_M(R_{MB,k}) \\ &= p_c + \frac{(2^{R_{MB,k}} - 1) N_0 B}{|H_{MB}|^2} \\ &\quad - R_{MB,k} \cdot \frac{\ln 2 \cdot 2^{R_{MB,k}} N_0 B}{|H_{MB,k}|^2} \end{aligned} \quad (81)$$

The first-order derivative of  $\beta(R_{MB,k})$  is

$$\beta'(R_{MB,k}) = -R_{MB,k} \cdot p''_M(R_{MB,k}). \quad (82)$$

The first-order and second-order derivatives of  $p_M(R_{MB,k})$  are both positive:

$$p'_M(R_{MB,k}) = \frac{\ln 2 \cdot 2^{R_{MB,k}} N_0 B}{|H_{MB,k}|^2} > 0, \quad (83)$$

$$p''_M(R_{MB,k}) = \frac{(\ln 2)^2 \cdot 2^{R_{MB,k}} N_0 B}{|H_{MB,k}|^2} > 0. \quad (84)$$

Substituting (84) into (82), we find that  $\beta'(R_{MB,k})$  is always negative, thus  $\beta(R_{MB,k})$  is monotonically decreasing. Then we consider the positive and negative characters of  $\beta(R_{MB,k})$ . For a brief representation, we use  $R$  to represent  $R_{MB,k}$  here. Using L'Hopital's rule, we have:

$$\beta(R) \Big|_{R \rightarrow 0} = p_c > 0, \quad (85)$$

$$\begin{aligned} \beta(R) \Big|_{R \rightarrow \infty} &= \lim_{R \rightarrow \infty} \frac{p_c + p_M(R) - R \cdot p'_M(R)}{R} \cdot R, \\ &= \lim_{R \rightarrow \infty} \frac{(p_c + p_M(R) - R \cdot p'_M(R))'}{R'} \cdot R \\ &= \lim_{R \rightarrow \infty} \frac{N_0 B}{|H_{MB}|^2} \frac{2^R \ln 2 - 2^R \ln 2 - R (\ln 2)^2 \cdot 2^R}{R} \cdot R \\ &= -R^2 \cdot p''_M(R) < 0. \end{aligned} \quad (86)$$

Note that  $(\cdot)'$  means the first-order derivative and  $(\cdot)''$  means the second-order derivative. Since  $\beta(R_{MB,k})$  is continuous and monotonically decreasing, it must go through the X positive half axis. Thus the root  $\tilde{R}_{MB,k}$  is positive. So we have  $\beta(R_{MB,k}) > 0$  for  $0 < R_{MB,k} < \tilde{R}_{MB,k}$ , and  $\beta(R_{MB,k}) < 0$  for  $R_{MB,k} > \tilde{R}_{MB,k}$ .

## APPENDIX C

### PROOF OF LEMMA 2

To prove that the objective function  $E(R_{MB,k})$  is concave, we need to prove that the Hessian matrix is non-positive, which is the second-order derivative of  $E(R_{MB,k})$ .

As shown in (23), the first-order derivative of  $E(R_{MB,k})$  is

$$\frac{\partial E(R_{MB,k})}{\partial R_{MB,k}} = \frac{p_c + p_M(R_{MB,k}) - R_{MB,k} \cdot p'_M(R_{MB,k})}{(p_M(R_{MB,k}) + p_c)^2}, \quad (87)$$

Then the second order derivative of  $E(R_{MB,k})$  is:

$$\begin{aligned} \frac{\partial^2 E(R_{MB,k})}{\partial R_{MB,k}^2} &= \frac{\beta'(R_{MB,k}) [p_M(R_{MB,k}) + p_c]^2}{[p_M(R_{MB,k}) + p_c]^4} \\ &\quad - \frac{2\beta(R_{MB,k}) [p_M(R_{MB,k}) + p_c] \cdot p'_M(R_{MB,k})}{[p_M(R_{MB,k}) + p_c]^4}, \forall k. \end{aligned} \quad (88)$$

When  $R_{MB,k} \leq \tilde{R}_{MB,k}$ , we have proved that  $\beta(R_{MB,k}) \geq 0$  in Appendix B. So  $\frac{\partial^2 E(R_{MB,k})}{\partial R_{MB,k}^2}$  is negative. So the Hessian matrix of  $E(R_{MB,k})$  is negative definite.  $E(R_{MB,k})$  is concave if the range of  $R_{MB,k}$  is set to be  $R_{MB,k} \leq \tilde{R}_{MB,k}$ .

In addition, as for  $R_{MB,k} > \tilde{R}_{MB,k}$ , we have proved that  $\beta(R_{MB,k}) < 0$  for  $R_{MB,k} > \tilde{R}_{MB,k}$  in Appendix B. So the first order of  $E(R_{MB,k})$  is negative. So  $E(R_{MB,k})$  is monotonically decreasing for  $R_{MB,k} > \tilde{R}_{MB,k}$ .

## APPENDIX D

### PROOF OF THEOREM 1

We prove Theorem 1 using reduction to absurdity.

*a:* Suppose that for  $k = a$ , the optimal solution is  $R_{MB,a}^* > R_0$ . Then one can always find a  $\bar{R}_{MB,a}$  satisfying  $R_0 < \bar{R}_{MB,a} < R_{MB,a}^*$  without violating any constraints of (P2). Referring to Lemma 2, we know that  $E(R_{MB,a})$  is monotonically decreasing for  $R_{MB,a} \geq R_0$ . So  $E(\bar{R}_{MB,a}) > E(R_{MB,a}^*)$ , which means that  $R_{MB,a}^*$  is not the optimal solution for  $E(R_{MB,a})$ . The inference violates the assumption. The assumption is wrong. Results should be  $R_{MB,a}^* = R_0$ .

*b:* Suppose that  $R_{MB,b}^* > \tilde{R}_{MB,b}$ . Then one can always find a  $\bar{R}_{MB,b}$ , satisfying  $\tilde{R}_{MB,b} < \bar{R}_{MB,b} < R_{MB,b}^*$  without violating any constraints of (P2). Referring to Lemma 2, we have  $E(R_{MB,b})$  monotonically decreasing for  $R_{MB,b} \geq \tilde{R}_{MB,b}$ . Then we have  $E(\bar{R}_{MB,b}) > E(R_{MB,b}^*)$ . It violates the assumption that  $R_{MB,b}^*$  is the optimal solution, thus the assumption is invalid. The optimal value should be  $R_{MB,b}^* \in [R_0, \tilde{R}_{MB,b}]$ .

So Theorem 1 is proved. The optimal results for  $E(R_{MB,a})$  is  $R_{MB,a}^* = R_0$ ; the optimal results for  $E(R_{MB,b})$  is  $R_{MB,b}^* \in [R_0, \tilde{R}_{MB,b}]$ .

## REFERENCES

- [1] Y. Zeng, X. Xu, and R. Zhang, "Trajectory design for completion time minimization in UAV-enabled multicasting," *IEEE Trans. Wireless Commun.*, vol. 17, no. 4, pp. 2233–2246, April 2018.
- [2] Z. Li, F. Xiao, S. Wang, T. Pei, and J. Li, "Achievable rate maximization for cognitive hybrid satellite-terrestrial networks with AF-relays," *IEEE J. Sel. Areas Commun.*, vol. 36, no. 2, pp. 304–313, Feb 2018.
- [3] Y. Li, L. Liu, H. Li, J. Zhang, and Y. Yi, "Resource allocation for delay-sensitive traffic over lte-advanced relay networks," *IEEE Trans. Wireless Commun.*, vol. 14, no. 8, pp. 4291–4303, Aug 2015.
- [4] S. Wang, R. Ruby, V. C. M. Leung, Z. Yao, X. Liu, and Z. Li, "Sum-power minimization problem in multisource single-af-relay networks: A new revisit to study the optimality," *IEEE Trans. Veh. Technol.*, vol. 66, no. 11, pp. 9958–9971, Nov 2017.
- [5] M. Mozaffari, W. Saad, M. Bennis, and M. Debbah, "Unmanned aerial vehicle with underlaid device-to-device communications: Performance and tradeoffs," *IEEE Trans. Wireless Commun.*, vol. 15, no. 6, pp. 3949–3963, June 2016.

- [6] K. Liu, "Outage performance of cooperative relaying with fixed and best-selected mobile relays over non-identically distributed links," *IEEE Wireless Commun. Lett.*, vol. 1, no. 5, pp. 548–551, October 2012.
- [7] A. Fotouhi, H. Qiang, M. Ding, M. Hassan, L. G. Giordano, A. Garcia-Rodriguez, and J. Yuan, "Survey on UAV cellular communications: Practical aspects, standardization advancements, regulation, and security challenges," *IEEE Comm. Surveys Tuts.*, vol. 21, no. 4, pp. 3417–3442, 2019.
- [8] P. Lindahl, E. Moog, and S. R. Shaw, "Simulation, design, and validation of an UAV SOFC propulsion system," *IEEE Trans. Aerosp. Electron. Syst.*, vol. 48, no. 3, pp. 2582–2593, JULY 2012.
- [9] M. Boukoberine, Z. Zhou, and M. Benbouzid, "A critical review on unmanned aerial vehicles power supply and energy management: Solutions, strategies, and prospects," *Applied Energy*, vol. 255, p. 113823, 2019.
- [10] K. Celik and H. Eren, "UAV fuel preferences for future cities," in *2018 6th International Istanbul Smart Grids and Cities Congress and Fair (ICSG)*, April 2018, pp. 151–154.
- [11] J. Kim, S. Kim, C. Ju, and H. I. Son, "Unmanned aerial vehicles in agriculture: A review of perspective of platform, control, and applications," *IEEE Access*, vol. 7, pp. 105 100–105 115, 2019.
- [12] H. Shakhtrah, A. H. Sawalmeh, A. Al-Fuqaha, Z. Dou, E. Almaita, I. Khalil, N. S. Othman, A. Khreishah, and M. Guizani, "Unmanned aerial vehicles (uavs): A survey on civil applications and key research challenges," *IEEE Access*, vol. 7, pp. 48 572–48 634, 2019.
- [13] Y. Wang, Y. Shi, M. Cai, W. Xu, T. Pan, and Q. Yu, "Study of fuel-controlled aircraft engine for fuel-powered unmanned aerial vehicle: Energy conversion analysis and optimization," *IEEE Access*, vol. 7, pp. 109 246–109 258, 2019.
- [14] J. Li, L. Zhou, Z. Zhao, X. Wang, and F. Zhang, "Research on knocking characteristics of kerosene spark-ignition engine for unmanned aerial vehicle (UAV) by numerical simulation," *Thermal Sci. Eng. Progress*, vol. 9, pp. 1 – 10, 2019. [Online]. Available: <http://www.sciencedirect.com/science/article/pii/S2451904918304748>
- [15] Q. Song, F. Zheng, Y. Zeng, and J. Zhang, "Joint beamforming and power allocation for UAV-enabled full-duplex relay," *IEEE Trans. Veh. Technol.*, vol. 68, no. 2, pp. 1657–1671, Feb 2019.
- [16] L. Xiao, X. Lu, D. Xu, Y. Tang, L. Wang, and W. Zhuang, "UAV relay in VANETs against smart jamming with reinforcement learning," *IEEE Trans. Veh. Technol.*, vol. 67, no. 5, pp. 4087–4097, May 2018.
- [17] F. Cheng, G. Gui, N. Zhao, Y. Chen, J. Tang, and H. Sari, "UAV-relaying-assisted secure transmission with caching," *IEEE Trans. Commun.*, vol. 67, no. 5, pp. 3140–3153, May 2019.
- [18] F. Ono, H. Ochiai, and R. Miura, "A wireless relay network based on unmanned aircraft system with rate optimization," *IEEE Trans. Wireless Commun.*, vol. 15, no. 11, pp. 7699–7708, Nov 2016.
- [19] P. Zhan, K. Yu, and A. L. Swindlehurst, "Wireless relay communications with unmanned aerial vehicles: Performance and optimization," *IEEE Trans. Aerosp. Electron. Syst.*, vol. 47, no. 3, pp. 2068–2085, July 2011.
- [20] K. Li, W. Ni, X. Wang, R. P. Liu, S. S. Kanhere, and S. Jha, "Energy-efficient cooperative relaying for unmanned aerial vehicles," *IEEE Trans. Mobile Comput.*, vol. 15, no. 6, pp. 1377–1386, June 2016.
- [21] A. Chamseddine, O. Akhrif, G. Charland-Arcand, F. Gagnon, and D. Couillard, "Communication relay for multigroup units with unmanned aerial vehicle using only signal strength and angle of arrival," *IEEE Trans. Contr. Syst. Technol.*, vol. 25, no. 1, pp. 286–293, Jan 2017.
- [22] M. Mozaffari, W. Saad, M. Bennis, Y. Nam, and M. Debbah, "A tutorial on UAVs for wireless networks: Applications, challenges, and open problems," *IEEE Commun. Surveys Tuts.*, vol. 21, no. 3, pp. 2334–2360, 2019.
- [23] H. Zhang, N. Liu, K. Long, J. Cheng, V. C. M. Leung, and L. Hanzo, "Energy efficient subchannel and power allocation for software-defined heterogeneous vlc and rf networks," *IEEE J. Sel. Areas Commun.*, vol. 36, no. 3, pp. 658–670, March 2018.
- [24] H. Zhang, B. Wang, C. Jiang, K. Long, A. Nallanathan, V. C. M. Leung, and H. V. Poor, "Energy efficient dynamic resource optimization in noma system," *IEEE Trans. Wireless Commun.*, vol. 17, no. 9, pp. 5671–5683, Sep. 2018.
- [25] H. Zhang, H. Liu, J. Cheng, and V. C. M. Leung, "Downlink energy efficiency of power allocation and wireless backhaul bandwidth allocation in heterogeneous small cell networks," *IEEE Trans. Commun.*, vol. 66, no. 4, pp. 1705–1716, April 2018.
- [26] Y. Zeng, R. Zhang, and T. J. Lim, "Wireless communications with unmanned aerial vehicles: Opportunities and challenges," *IEEE Commun. Mag.*, vol. 54, no. 5, pp. 36–42, May 2016.
- [27] C. H. Liu, Z. Chen, J. Tang, J. Xu, and C. Piao, "Energy-efficient UAV control for effective and fair communication coverage: A deep reinforcement learning approach," *IEEE J. Sel. Areas Commun.*, vol. 36, no. 9, pp. 2059–2070, Sep. 2018.
- [28] D. Yang, Q. Wu, Y. Zeng, and R. Zhang, "Energy tradeoff in ground-to-UAV communication via trajectory design," *IEEE Trans. Veh. Technol.*, vol. 67, no. 7, pp. 6721–6726, July 2018.
- [29] Y. Zeng and R. Zhang, "Energy-efficient UAV communication with trajectory optimization," *IEEE Trans. Wireless Commun.*, vol. 16, no. 6, pp. 3747–3760, June 2017.
- [30] *Propagation data and prediction methods for the design of terrestrial broadband millimetric radio access systems*, ITU P Series, Radiowave Propagation, Rec. P.1410-2, Rev. Burlington, MA, 2003.
- [31] A. Al-Hourani, S. Kandeepan, and S. Lardner, "Optimal LAP altitude for maximum coverage," *IEEE Wireless Commun. Lett.*, vol. 3, no. 6, pp. 569–572, Dec 2014.
- [32] R. Ma, W. Yang, Y. Zhang, J. Liu, and H. Shi, "Secure mmWave communication using UAV-enabled relay and cooperative jammer," *IEEE Access*, vol. 7, pp. 119 729–119 741, 2019.
- [33] H. Kang, J. Joung, and J. Kang, "A study on probabilistic Line-of-Sight Air-to-Ground channel models," in *2019 34th Int. Tech. Conf. Circuits/Syst., Comput. Commun. (ITC-CSCC)*, June 2019, pp. 1–2.
- [34] M. Alzenad, A. El-Keyi, and H. Yanikomeroglu, "3-D placement of an unmanned aerial vehicle base station for maximum coverage of users with different QoS requirements," *IEEE Wireless Commun. Lett.*, vol. 7, no. 1, pp. 38–41, Feb 2018.
- [35] W. Mei and R. Zhang, "Uplink cooperative NOMA for cellular-connected UAV," *IEEE J. Sel. Topics. Signal Process.*, vol. 13, no. 3, pp. 644–656, June 2019.
- [36] Q. Wu, Y. Zeng, and R. Zhang, "Joint trajectory and communication design for multi-UAV enabled wireless networks," *IEEE Trans. Wireless Commun.*, vol. 17, no. 3, pp. 2109–2121, March 2018.
- [37] Y. Zeng, J. Xu, and R. Zhang, "Energy minimization for wireless communication with rotary-wing UAV," *IEEE Trans. Wireless Commun.*, vol. 18, no. 4, pp. 2329–2345, April 2019.
- [38] Y. Zeng, R. Zhang, and T. J. Lim, "Throughput maximization for UAV-enabled mobile relaying systems," *IEEE Trans. Commun.*, vol. 64, no. 12, pp. 4983–4996, Dec 2016.
- [39] A. Filippone, *Flight Performance of Fixed and Rotary Wing Aircraft*. Lincoln House, Jordan Hill: Butterworth-Heinemann, 2006.
- [40] Y. Sun, D. Xu, D. W. K. Ng, L. Dai, and R. Schober, "Optimal 3D-trajectory design and resource allocation for solar-powered UAV communication systems," *IEEE Trans. Commun.*, vol. 67, no. 6, pp. 4281–4298, June 2019.
- [41] J. Seddon and S. Newman, *Basic Helicopter Aerodynamics*, 3rd ed. West Sussex, UK: John Wiley and Sons, 2011.
- [42] C. You and R. Zhang, "3D trajectory optimization in rician fading for UAV-enabled data harvesting," *IEEE Trans. Wireless Commun.*, vol. 18, no. 6, pp. 3192–3207, June 2019.
- [43] G. Zhang, Q. Wu, M. Cui, and R. Zhang, "Securing UAV communications via joint trajectory and power control," *IEEE Trans. Wireless Commun.*, vol. 18, no. 2, pp. 1376–1389, 2019.
- [44] Q. Hu, Y. Cai, G. Yu, Z. Qin, M. Zhao, and G. Y. Li, "Joint offloading and trajectory design for UAV-enabled mobile edge computing systems," *IEEE Internet Things J.*, vol. 6, no. 2, pp. 1879–1892, 2019.



**Tong Zhang** received the B.S. degree in communication engineering from the Harbin Institute of Technology, Weihai, China, in 2018. She is currently pursuing the Ph.D. degree in communication engineering with the Harbin Institute of Technology, Harbin, China. Her research interests include UAV communications and non-orthogonal multiple access.



**Gongliang Liu** was born in Shandong, China, in 1979. He received the B.S. degree in measuring and control technology and instrumentations and M.Eng. and Ph.D. degrees in electrical engineering from the Harbin Institute of Technology, Harbin, China, in 2001, 2003, and 2007, respectively. He was a Visiting Scholar with The University of British Columbia, Canada, from 2015 to 2016. He is currently a Professor with the Harbin Institute of Technology, Weihai. His current interests include wireless communications and networking.



**Arumugam Nallanathan** (S'97-M'00-SM'05-F'17) is Professor of Wireless Communications and Head of the Communication Systems Research (CSR) group in the School of Electronic Engineering and Computer Science at Queen Mary University of London since September 2017. He was with the Department of Informatics at King's College London from December 2007 to August 2017, where he was Professor of Wireless Communications from April 2013 to August 2017 and a Visiting Professor from September 2017. He was an Assistant Professor in the Department of Electrical and Computer Engineering, National University of Singapore from August 2000 to December 2007. His research interests include Artificial Intelligence for Wireless Systems, Beyond 5G Wireless Networks, Internet of Things (IoT) and Molecular Communications. He published nearly 500 technical papers in scientific journals and international conferences. He is a co-recipient of the Best Paper Awards presented at the IEEE International Conference on Communications 2016 (ICC'2016), IEEE Global Communications Conference 2017 (GLOBECOM'2017) and IEEE Vehicular Technology Conference 2018 (VTC'2018). He is an IEEE Distinguished Lecturer. He has been selected as a Web of Science Highly Cited Researcher in 2016.

He is an Editor for IEEE Transactions on Communications and Senior Editor for IEEE Wireless Communications Letters. He was an Editor for IEEE Transactions on Wireless Communications (2006-2011), IEEE Transactions on Vehicular Technology (2006-2017) and IEEE Signal Processing Letters. He served as the Chair for the Signal Processing and Communication Electronics Technical Committee of IEEE Communications Society and Technical Program Chair and member of Technical Program Committees in numerous IEEE conferences. He received the IEEE Communications Society SPCE outstanding service award 2012 and IEEE Communications Society RCC outstanding service award 2014.



2017, and IEEE ComSoc Asia-Pacific Best Young Researcher Award in 2019.

**Haijun Zhang** (M'13, SM'17) is currently a Full Professor in University of Science and Technology Beijing, China. He was a Postdoctoral Research Fellow in Department of Electrical and Computer Engineering, the University of British Columbia (UBC), Canada. He serves as an Editor of IEEE Transactions on Communications, IEEE Transactions on Green Communications Networking, and IEEE Communications Letters. He received the IEEE CSIM Technical Committee Best Journal Paper Award in 2018, IEEE ComSoc Young Author Best Paper Award in 2017, and IEEE ComSoc Asia-Pacific Best Young Researcher Award in 2019.



**Wenjing Kang** received the B.S., M.Eng., and Ph.D. degrees from the Harbin Institute of Technology, Harbin, China, in 2001, 2004, and 2007, respectively, all in measuring and control technology and instrumentations. She is currently an Assistant Professor with the Harbin Institute of Technology, Weihai, China. Her research interests include visual tracking and wireless networks.



**George K. Karagiannidis** (M'96-SM'03-F'14) was born in Pithagorion, Samos Island, Greece. He received the University Diploma (5 years) and PhD degree, both in electrical and computer engineering from the University of Patras, in 1987 and 1999, respectively. From 2000 to 2004, he was a Senior Researcher at the Institute for Space Applications and Remote Sensing, National Observatory of Athens, Greece. In June 2004, he joined the faculty of Aristotle University of Thessaloniki, Greece where he is currently Professor in the Electrical & Computer

Engineering Dept. and Head of Wireless Communications Systems Group (WCSG). He is also Honorary Professor at South West Jiaotong University, Chengdu, China. His research interests are in the broad area of Digital Communications Systems and Signal processing, with emphasis on Wireless Communications, Optical Wireless Communications, Wireless Power Transfer and Applications and Communications & Signal Processing for Biomedical Engineering. Dr. Karagiannidis has been involved as General Chair, Technical Program Chair and member of Technical Program Committees in several IEEE and non-IEEE conferences. In the past, he was Editor in several IEEE journals and from 2012 to 2015 he was the Editor-in Chief of IEEE Communications Letters. Currently, he serves as Associate Editor-in Chief of IEEE Open Journal of Communications Society. Dr. Karagiannidis is one of the highly-cited authors across all areas of Electrical Engineering, recognized from Clarivate Analytics as Web-of-Science Highly-Cited Researcher in the five consecutive years 2015-2019.